(1)

SEMI-ANNUAL REPORT

"CHARACTERIZATION OF RAPIDLY SOLIDIFIED ALLOYS"

D. SHECHTMAN AND E. HOROWITZ

THE JOHNS HOPKINS UNIVERSITY
CENTER FOR MATERIALS RESEARCH
BALTIMORE, MARYLAND 21218
(301-338-7916)

DARPA ORDER NO.: MDA 903- 1-C-0555
EFFECTIVE DATE: 08-01-81
EXPIRATION DATE: 07-31-83
SPONSORED BY: DEFENSE ADVANCED RESEARCH PROJECTS AGENCY (DARPA)

FEBRUARY 1983

TABLE OF CONTENTS

FIGURES

FIGURES

FIGURES

FIGURES

EXECUTIVE SUMMARY

This report discusses the research performed on the DARPA program since the last semi-annual progress report. Periodic quarterly progress reports and special reports have been submitted to DARPA, but this document interrelates and correlates the work accomplished to date in a unified manner. The studies included in this report cover various microstructural aspects of rapid solidification of metallic systems which are based on aluminum (Aℓ-Fe, Aℓ-Mn, and Aℓ-Cu), silver base (Ag-Cu) and the quasibinary eutectic NiAℓ-Cr. The results of these investigations have been presented in a series of presentations,* four of which were given at the Third Conference on Rapid Solidification Processing: Principles and Technologies, National Bureau of Standards, Gaithersburg, Md., on December 6-8, 1982. One presentation on the metastable phases in rapidly solidified aluminum-rich Aℓ-Fe alloys was given at the Annual Materials Research Society meeting on November 1-4, 1982, in Boston, Massachusetts. Several papers describing the various results obtained are in preparation for the open scientific literature.

*See list of publications in Appendix 1.

I. The Microstructure of Rapidly Solidified NiAℓ-Cr Quasibinary Eutectic

Introduction

This study was done in cooperation with W. J. Boettinger and F. S. Biancaniello of the Metallurgy Division of NBS and T. Z. Kattamis of the Department of Metallurgy, University of Connecticut.

The NiAℓ-Cr quasibinary eutectic has some unique properties that make it attractive for a microstructural study. The α-Cr phase of the eutectic has a BCC structure, the β NiAℓ phase a CsCℓ (ordered BCC) structure, and both phases have a similar lattice parameter in equilibrium. This results in a very low surface tension between the phases which produces a fine eutectic microstructure. Rapid solidification studies of this eutectic are therefore expected to indicate an extended solid solubility or an extremely fine eutectic.

The directional solidification of NiAℓ-Cr quasibinary eutectic alloy (Ni-33at%Aℓ-34at%Cr) was previously investigated by Walter, et al. [1-4],* who saw in it potential for high temperature applications. The eutectic consists of fine, nonfaceted fibers of α-Cr BCC phase embedded in a β-NiAℓ matrix, which is an ordered BCC phase (CsCℓ-type) containing some chromium in solid solution. From previous work by Kornilov, et al. [5], the NiAℓ-Cr quasibinary eutectic temperature is 1445°C. The α-Cr phase at 1200°C contains 20.6 mole% NiAℓ and, hence, has a composition of 17.1at%Ni-17.1at%Aℓ-65.8at%Cr. The β-NiAℓ

*See references on p. 20.

phase at 1200°C contains 84.5 mole% NiAℓ, hence has a composition of 45.8at%Ni-45.8%Aℓ-8.4at%Cr. The volume fraction of fibers is about 0.34. In the directionally solidified eutectic all directions and planes of the two phases are parallel. The solidification microstructure consists of eutectic colonies of α-fibers of circular cross-section embedded in <100>-oriented columnar grains of β-NiAℓ and parallel to the growth direction, except near the cell boundaries where they are inclined to this direction. Despite this inclination the crystallographic relationship between fibers and matrix remains the same [1]. Both cubic phases are crystallographically related with only a small lattice mismatch, as evidenced by the large distance between dislocations observed at the interphase interface.

Walter, et al. [2] studied the effect of growth velocity on inter-fiber spacing. They quantitatively established the decrease in cell size and inter-fiber spacing with increasing growth velocity. They also investigated the effect of alloy additions on microstructural changes, in particular the rod-to-plate transition [3].

It appeared interesting to extend the study of solidification microstructures of the NiAℓ-Cr quasibinary eutectic to those achieved by rapid solidification, anticipating that the small difference in lattice parameter between the two phases would lead to substantial extension in solid solubility. Melt-spinning was used in this investigation. The growth rates achieved in this process are difficult to quantify, because of

the possibility of bulk undercooling and an imprecise knowledge of the interface heat transfer coefficient. However, melt-spinning provides a simple way to assess the alloy's response to rapid solidification processing.

Results of the work on microstructure of melt-spun ribbon of NiAℓ-Cr quasibinary eutectic alloy are reported herein and are also included in another publication [6].

Experimental Procedure

Rapidly solidified ribbons of NiAℓ-Cr quasibinary eutectic were melt-spun on a room temperature wheel in a helium atmosphere. Ribbons of about 25μm thick and 2.5mm wide were obtained at a linear velocity of 24 m/s. The ribbons were studied by optical microscopy, X-ray diffraction and analytical electron microscopy. Specimens for electron microscopy were electropolished and studied in a scanning transmission electron microscope equipped for nondispersive X-ray fluorescence analysis. The composition of the phases in the foil was evaluated by using the nominal composition of the specimen as standard. The Cliff-Lorimer coefficients were determined by using the intensities obtained from a thin area representing the general microstructure with a probe size of about 1μm. Analysis of individual phases was then conducted in the same area of similar thickness. The C-L coefficients were redetermined for each set of analyses in different regions of the foil. This procedure eliminates the need for additional corrections of the measured X-ray intensities.

Results

The microstructure of an arc-melted chill-cast cylindrical specimen, 6.3mm in diameter is illustrated in Figure 1. The rod-like α-Cr-rich phase is revealed as the dark etching phase.

The cast microstructure of the ribbons consists mainly of a columnar zone with columnar grains parallel to the heat flow direction. The intergranular spaces were not optically resolved. The average columnar grain width increased slightly with distance from the chill, Figure 2, from about 0.5 to 1.3μm. The average columnar grain width also increased slightly with ribbon thickness.

The microstructure of the ribbon as observed by electron microscopy is shown in Figure 3, which represents cross-sections of columnar grains that grew perpendicular to the ribbon surface. The columnar grains average 0.5μm in diameter and are surrounded by a fine eutectic. The boundary between a columnar grain and a region of particularly fine eutectic is shown at a higher magnification in Figure 4. The columnar grain is decomposed into a fine microstructure typical of conditional spinodal decomposition [7] with an average wavelength of 10 nm (lower right, Figure 4). The eutectic rods grow roughly perpendicular to the columnar grain and their spacing ranges from 12nm, Figure 4, to 60nm, Figure 3. The microstructure is not uniform and in areas the volume fraction of the columnar grains by far exceeds that of the eutectic, Figure 5. In other regions of the same foil the volume fraction of the eutectic is much higher, Figure 6.

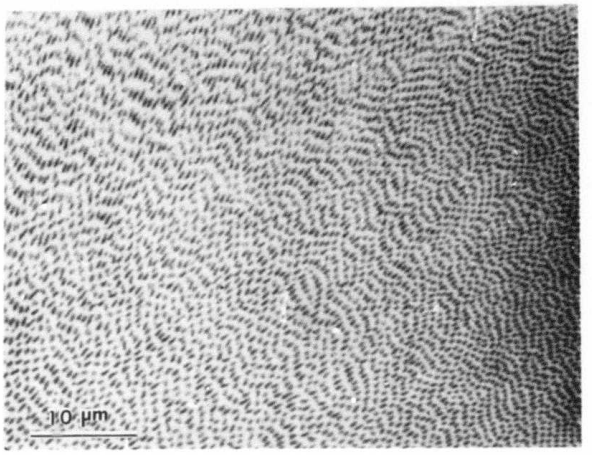

Figure 1: As-cast microstructure of arc-melted NiAl-Cr quasibinary eutectic (optical microscopy).

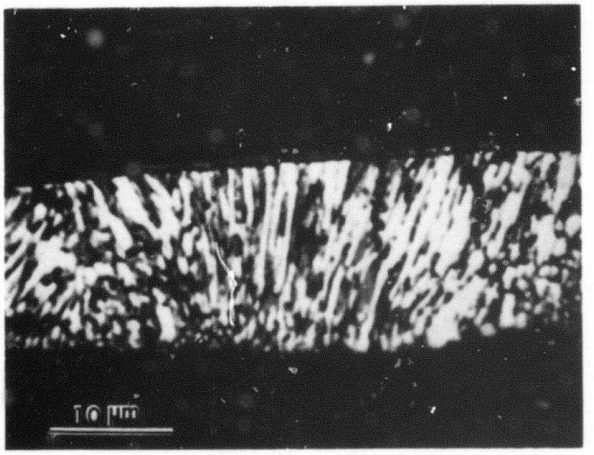

Figure 2: Columnar grains in melt-spun ribbon, edge-on section (optical microscopy).

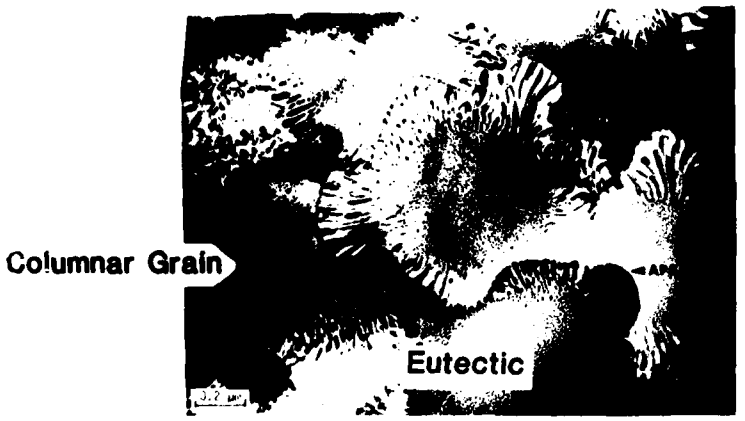

Figure 3: Transverse section of columnar grains and surrounding eutectic in melt-spun ribbon (TEM). Note APBS in center grain.

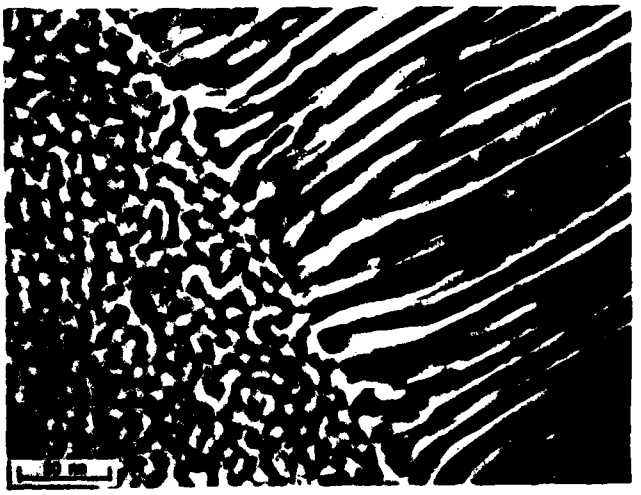

Figure 4: Columnar grain-eutectic interface. Inter-rod eutectic spacing: 12 nm (TEM).

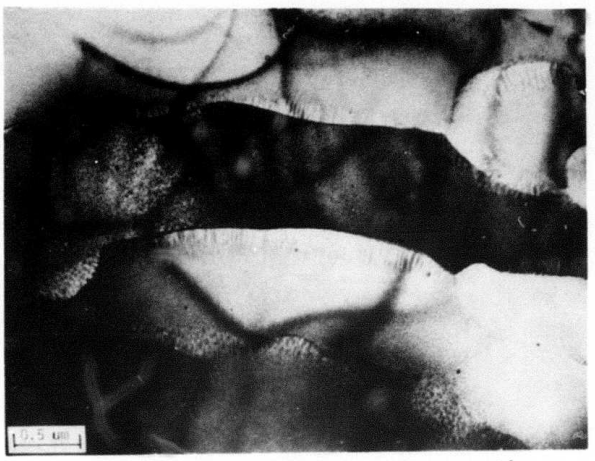

Figure 5: Region of foil consisting primarily of columnar grains (TEM).

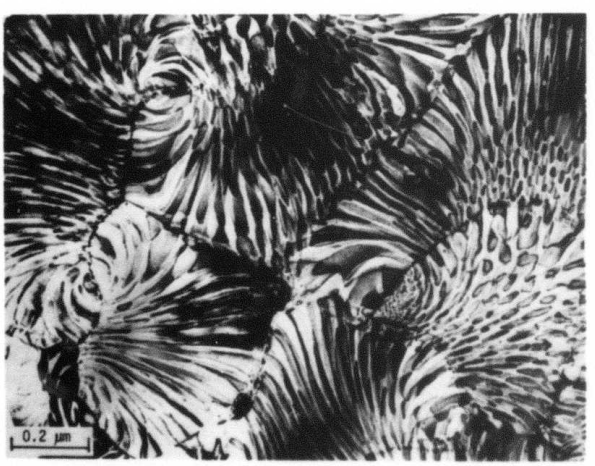

Figure 6: Region of foil consisting primarily of eutectic (TEM).

These variations may correspond to different distances from the heat sink, however, this was not confirmed in the present study.

A large proportion of columnar grains are single ordered domains. However, some of them contain two or more domains. Anti-phase domain boundaries are shown in Figures 3 and 7. These APBS run across the grain and in most cases end in a chromium-rich rod of the eutectic. The significance of these APBS to the understanding of the solidification process will be discussed later in this report.

A diffraction pattern taken from a columnar grain, Figure 8, identified the structure as CsCℓ (B2). A diffraction pattern taken from a columnar grain and its surrounding eutectic, Figure 9, shows no extra reflections besides the CsCℓ. This indicates that both phases in the eutectic and the columnar grain have the same orientation and almost identical lattice parameters. An X-ray diffraction scan taken from the ribbon shows that the reflections from the CsCℓ lattice and those from the BCC lattice are indistinguishable. Lattice parameter measurements resulted in a figure of a = 0.28882 nm. Microdiffraction patterns were taken from a rod and the adjacent matrix of the eutectic, as shown in Figure 10. The rod is identified as BCC, Figure 10a, the matrix as CsCℓ structure, Figure 10b.

A composition analysis of the columnar grain cores has shown that they have the same composition as the original alloy, Figures 11a and b. They are, therefore, β-NiAℓ supersaturated with chromium to the eutectic composition.

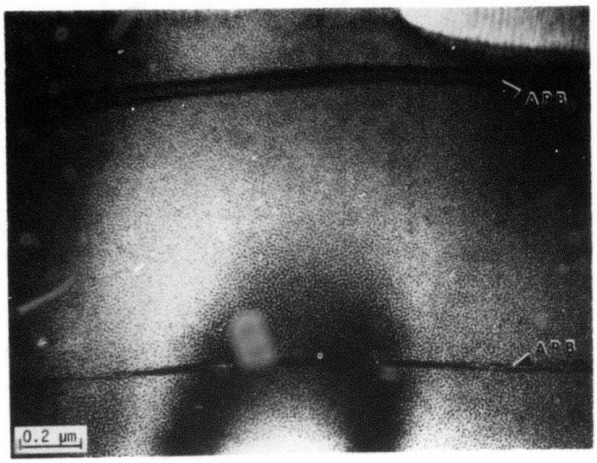

Figure 7:

High magnification illustration of APBS

Figure 8: Selected area diffraction (SAD) pattern of a columnar grain.

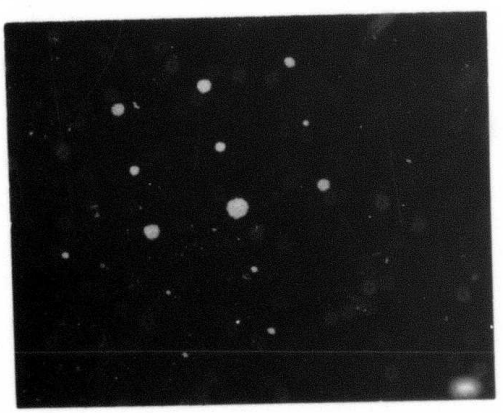

Figure 9: Diffraction pattern taken from a columnar grain and its surrounding eutectic.

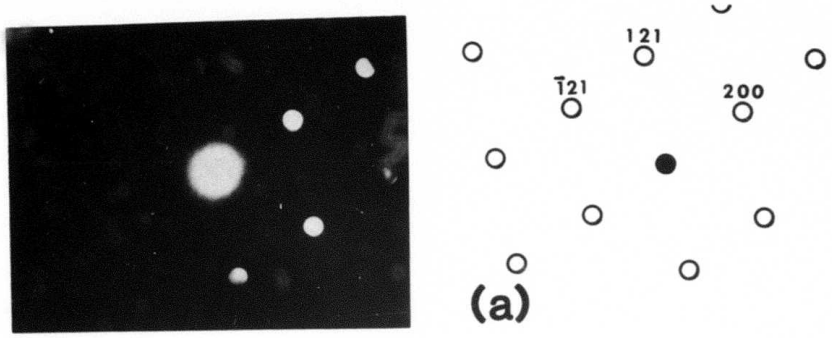

Figure 10: (a) Microdiffraction from rod in eutectic.
(b) Microdiffraction of matrix in eutectic.

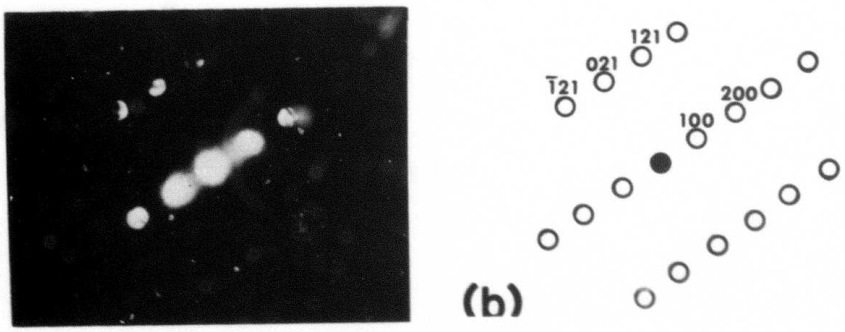

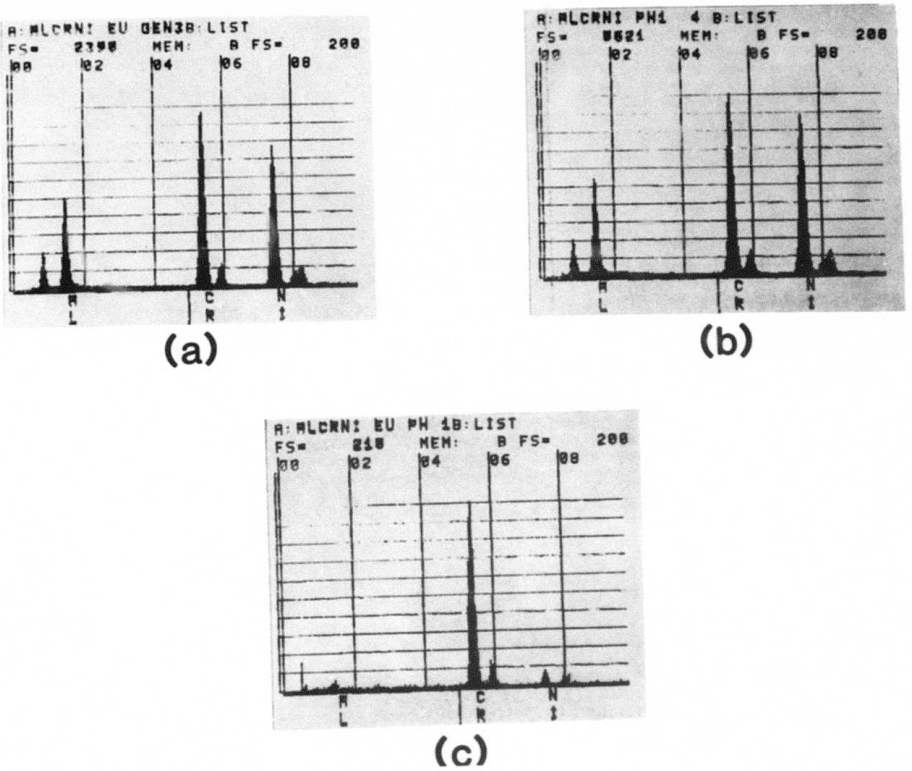

(a) (b) (c)

Figure 11: (a) General composition of the ribbon (used as standard). Composition of a columnar grain (b) and of a Cr rod in the eutectic (c).

The BCC phase in the eutectic was also analyzed, Figure 11c, and was found to be composed mainly of chromium of near equilibrium composition at the eutectic temperature (13.9 at%Ni and 7.5 at%Aℓ). The CsCℓ phase in the eutectic was not analyzed due to experimental difficulties, but based on an estimated volume fraction of the phases in the eutectic the phase is estimated to contain about 13 at% chromium, i.e., near the expected equilibrium composition for the β-NiAℓ phase at the eutectic temperature.

Discussion

Two features of this rapidly solidified structure are unique and will be discussed separately: the columnar grains of spinodally decomposing alloy with the β-NiAℓ structure and with composition near the eutectic, and the fine rod-type eutectic structure. It is important for the analysis of rapid solidification processes to establish whether the β-NiAℓ phase was a direct product of solidification or whether it has ordered in the solid state from a supersaturated α-Cr phase.

Columnar Grains

Because of the extension of solubility required for the formation of the columnar grains, an examination of the possible T_o curves for the NiAℓ-Cr system is in order. Figure 12 shows the stable phase diagram as solid lines [5] and a possible schematic set of metastable extensions of the solvus curves (dashed) and the T_o curves (long-short dashed). The

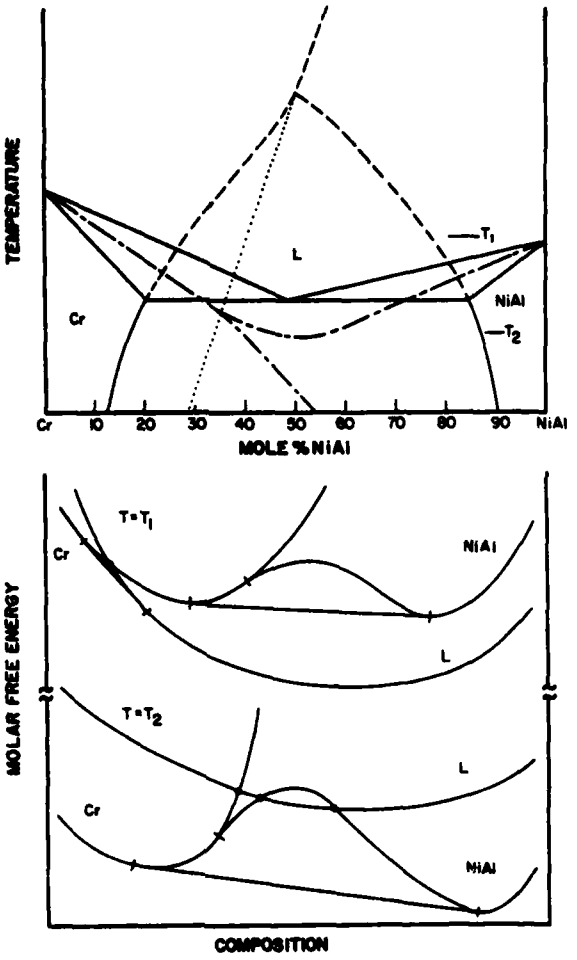

Figure 12: (a) NiAl-Cr phase diagram (solid lines), metastable extension of solvus curves (dashed) to tricritical point and T_o curves for α-Cr and β-NiAl. (b) Schematic free energy vs composition curves for NiAl-Cr system.

figure assumes that the two solvus curves meet at a metastable tricritical point above which the transition from the BCC phase to the CsCℓ phase is second order. This transformation can be second order according to the symmetry restrictions of Landau [8]. This metastable extension upward to the tricritical point, where the crystal structures differ by an ordering reaction, is formally similar to the metastable extension of the solvus curves between identical crystal structures (FCC) in the Ag-Cu system upward to an ordinary critical point. The proposed metastable tricritical point is thermodynamically identical to the stable tricritical point in the Fe-Aℓ system where the ordering is between Fe (BCC) and FeAℓ (B2) [7]. The schematic free energy curves for the solid phases shown in Figure 12 are identical to those proposed by Allen and Cahn [7]. With the addition of the liquid free energy curve to generate the stable eutectic phase diagram the structure of the T_o curves becomes apparent. In this figure we have assumed that the tricritical temperature is relatively low due to the similarity in the lattice parameters of β-NiAℓ and α-Cr. The lattice parameters would be identical above the tricritical point. In Figure 12 the dotted curve is the metastable extension of the second order phase transition below the tricritical point and is the locus of points where the free energy curves of the disordered and ordered phases join tangentially. This curve is generally thought to lie much closer to the solvus

for the disordered phase rather than that for the ordered phase [7]. The T_o curve for the disordered phase is seen to split into two branches when it crosses this dotted line. The lower branch is the continuation for the disordered phase, while the upper branch is for β-NiAℓ phase. This upper branch continues to the NiAℓ side of the diagram where it is the normal T_o curve for β-NiAℓ. The relatively small depression of the T_o curve for β-NiAℓ below the eutectic temperature is a consequence of the relatively low tricritical temperature. This fact again is formally similar to the T_o curve for Ag-Cu.

This diagram leads to two important conclusions which are consistent with the experimental results. First, the T_o curve for β-NiAℓ phase at the eutectic composition occurs at a higher temperature than the T_o curve for the α-Cr phase. Second, if the β-NiAℓ phase was formed with the eutectic composition directly from the melt, it would undergo subsequent solid state spinodal decomposition into ordered and disordered phases. This type of spinodal has been termed a conditional spinodal [7]. Typical decomposition structures of FeAℓ by conditional spinodal show coarse antiphase domains of the FeAℓ along with a fine scale compositional separation into disordered Fe and ordered phase.

The structure of the columnar grains in the present work is identical to the above mentioned structure. The grains

contain coarse antiphase domains and fine spinodal structure. This strongly suggests that the columnar grains solidified from the melt as supersaturated β-NiAℓ rather than supersaturated α-Cr. No antiphase domain boundaries would be visible, if the supersaturated Cr phase has solidified from the melt. The solidification of the ordered phase directly from the melt is also suggested by the fact that at the eutectic composition T_o for the ordered phase is higher than for the disordered phase. Hence, at the eutectic composition partitionless solidification of the β-NiAℓ phase can occur with less undercooling than that required for the partitionless solidification of the Cr phase.

Eutectic Structure

The solidification of the ribbon is envisioned in two steps. First, the formation of the columnar grains of supersaturated β-NiAℓ by partitionless solidification followed by the formation of a fine rod eutectic structure in the regions between the columnar grains by near equilibrium solidification. This eutectic solidification would presumably result from the reduction in growth rate caused from the evolution of latent heat during growth of columnar grains. The nucleation of the BCC phase from the CsCℓ phase seems to be difficult and is demonstrated by the fact that in most cases the eutectic originating from one columnar grain impinges directly upon an adjacent columnar grain. Only rarely do eutectics originating from

adjacent grains meet. Once the eutectic has nucleated it rapidly consumes the liquid that remains between the two columns.

The eutectic solidification apparently occurs with near equilibrium compositions for the two solid phases. Although a wide variety of eutectic spacings are seen ranging from 60nm down to 12nm the minimum spacings are of particular interest. As described by Boettinger [9] the temperature dependence of the liquid diffusion coefficient leads to a predicted maximum solidification rate for eutectics typically around 10 cm/s. In Ag-Cu eutectic alloys the maximum observed growth rate is 2.5 cm/s with a eutectic spacing of about 20nm [10]. Hence, the present observation of 12nm spacing is very interesting. Cline and Walter [2] have measured the rod spacing, λ, as a function of solidification velocity, v, up to 0.021 cm/s. They found these parameters to be related by $\lambda^2 = v7 \times 10^{-12} cm^3/s$, deduced from their graph. The value of the $\lambda^2 v$ constant for NiAl-Cr is smaller than for Ag-Cu ($1.4 \times 10^{-11} cm^3/s$) and for most other eutectics [11], presumably because of the low interface energy between β-NiAl and α-Cr phases, that can be attributed to the strong orientation relation and similarity of lattice parameters of the two phases in the eutectic. An experimental determination of the maximum growth rate of the NiAl-Cr eutectic structure will be performed in the future, using electron beam melting experiments.

References

[1] J. L. Walter, H. E. Cline and E. F. Koch, Trans. TMS-AIME, 245 (1969) 2073.

[2] J. L. Walter and H. E. Cline, Met. Trans., 1 (1970) 1221.

[3] H. E. Cline and J. L. Walter, Met. Trans., 1 (1970) 2907.

[4] J. L. Walter and H. E. Cline, Met. Trans., 4 (1973) 33.

[5] I. I. Kornilov and R. C. Mintz, Dokl. Akad. Nauk USSR, 94 (1954) 1085.

[6] D. Shechtman, T. Z. Kattamis, F. S. Biancaniello and W. J. Boettinger, to be published, J. Mater. Sci.

[7] S. M. Allen and J. W. Cahn, Acta Met., 24 (1976) 425.

[8] L. D. Landau and E. M. Lifshitz, Statistical Physics, Pergamon Press, London, 1958, p. 434.

[9] W. J. Boettinger, Rapidly Solidified Amorphous and Crystalline Alloys, B. H. Kear, B. C. Giessen and M. Cohen, ed., Elsevier Publishing Company, 1982, p. 15.

[10] W. J. Boettinger, R. Schaefer, F. Biancaniello and D. Shechtman, these Proceedings.

[11] W. Kurz and D. J. Fisher, International Metals Reviews, Nos. 5 and 6 (1979) 177.

II. Microstructural Studies on Supercooled Submicrometer Size Particles

Introduction

This study was performed in collaboration with S. D. Ridder and R. Mehrabian of NBS and is aimed at understanding some fundamental aspects of rapid solidification of alloy powders.

The use of electrohydrodynamics (EHD) in the atomization of metal alloys, in an apparatus hereafter referred to as the micro-particle processor (MPP) has provided a means of producing small quantities of submicrometer size metal particles. These small powders are, in general, transparent to 100 Kev electrons, used in conventional TEM analysis allowing a three-dimensional view of the entire solidification structure. This section will discuss some aspects of the microstructures observed in aluminum alloy powders produced by this process. Of particular interest here is the formation of metastable solid solutions in many of these powders and powders showing a transition from partitionless (massive) solidification to a segregated solidification mode as described in an earlier paper by Levi and Mehrabian [1].* The influence of particle size and composition on microstructure is discussed, especially as they relate to the apparent supercoolings achieved prior to nucleation in these particles.

*See references on p. 34.

The Microparticle Processor

This unique machine was developed by the Phrasor Company, Duarte, California. The principles on which it is based and the scope of its applications have been discussed in a number of papers and reports [2-12]. The machine uses an electrical potential difference of 10 to 20 Kv between a fine droplet of molten metal situated at a tip of a ceramic tube (Fig. 1) and a coplanar extractor electrode. A stream of fine particles is formed when the fine stream of molten metal is broken into droplets. The particles are collected on a replicating tape and are ready for microstructural study in the STEM following a simple preparation procedure.

The molten droplets are cooled by radiation only (the process is done in vacuum) and the cooling rate is thus inferior to that obtained by convection. Nevertheless, large undercooling of the molten droplets can be obtained. The cooling rates prior to the solidification of a given droplet, other factors being the composition, particle size and the temperature at which nucleation occurs. This undercooling in turn determines the relative size of the "rapidly solidified" portion of the particle, which solidifies virtually adiabatically [1].

The size distribution of the microparticles obtained at NBS ranges from about 3nm to 2μm. Larger particles, although formed are not solid when they reach the end of the path and

FIGURE 1.

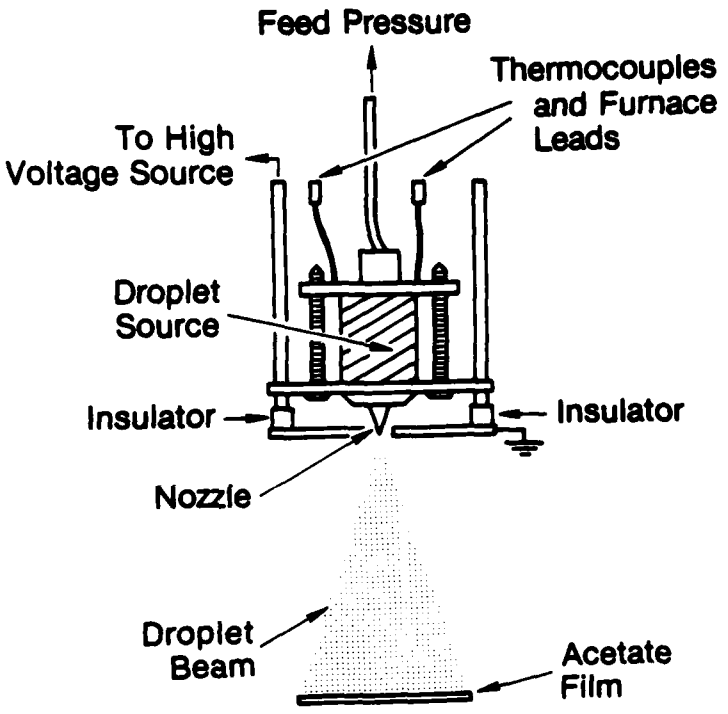

Figure 1. The Microparticle Processor.

and are thus splat on arrival. There are two major advantages in this distribution. First, a large proportion of the particles are transparent to the electron beam in the TEM (depending upon alloy composition) and second, the particles contain a range of microstructures generated by the various cooling rates.

Experimental Procedure

Various Aℓ-Cu binary alloy powders were produced by the microparticle processor (MPP) at NBS. The alloys contain 0.5, 1, 2, 3, 4.5 and 6 weight percent copper. The production parameters were 14 kv extraction voltage with an argon feed pressure of 50mm Hg cm^{-2} against a vacuum of 10^{-5}mm Hg cm^{-2}. The flight distance to the cellulose acetate tape collector was 150mm. Specimens for transmission electron microscopy were prepared by a deposition of a thin carbon layer on the particles carrying tape and the subsequent dissolving of the tape in acetone. Specimens thus made were mounted on 400 mesh grids and studied in a scanning transmission electron microscope (STEM) equipped with a non-dispersive x-ray analysis system. The study of composition variation in the particles involves several experimental difficulties, including the proper geometrical positioning of the particle relative to the grid base, the electron beam and the detector. Appropriate adjustments were made to compensate for these so as to produce minimum experimental error. Other difficulties are inherent to the shape and size of the individual particles under study. These

require a correction procedure that will take into account the specific electron beam location on the particle, i.e., the cross-section of the particle at that point and its location relative to the x-ray detector. Such a correction procedure was not used and only a thin foil composition determination procedure was performed. This may account for some inaccuracies in the composition analysis.

In situ heat treatments of individual powder particles were performed under a controlled electron beam in the STEM and the sequence of precipitation was recorded.

Results

The particles observed are spherical and their size varies between 3nm and 2μm. Larger particles do not solidify before hitting the carrying tape. The microstructure of individual powder particles of various compositions is given in Fig. 2. Two kinds of microstructure have been observed. The first is characterized by partitionless solidification. Such particles contain up to 2 wt % Cu and also particles smaller than 1μm that contain 3 wt % Cu. Particles that contain 4.5 and 6 wt % Cu can also solidify in a partitionless regime provided that they are smaller than 0.5μm. Larger particles and ones which contain 3 wt % Cu and are larger than 1μm exhibit another form of solidification characterized by segregated cell structure.

The Cu concentration as a function of the distance from the interface between the partitionlesss and segregated regions is shown in Fig. 3b while 3a indicates the points

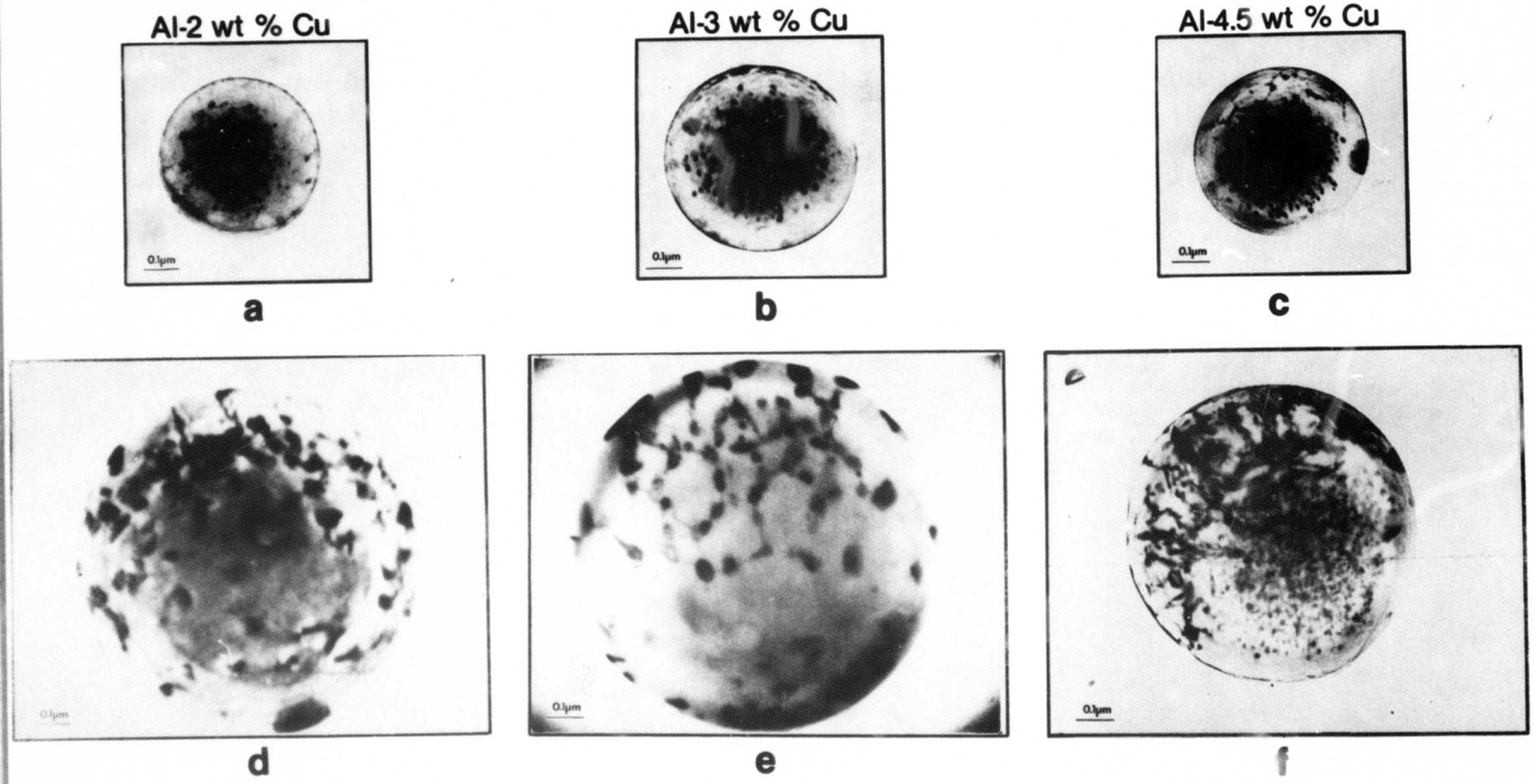

Figure 2. The microstructure of Aℓ-Cu powder particles as a function of size and composition.

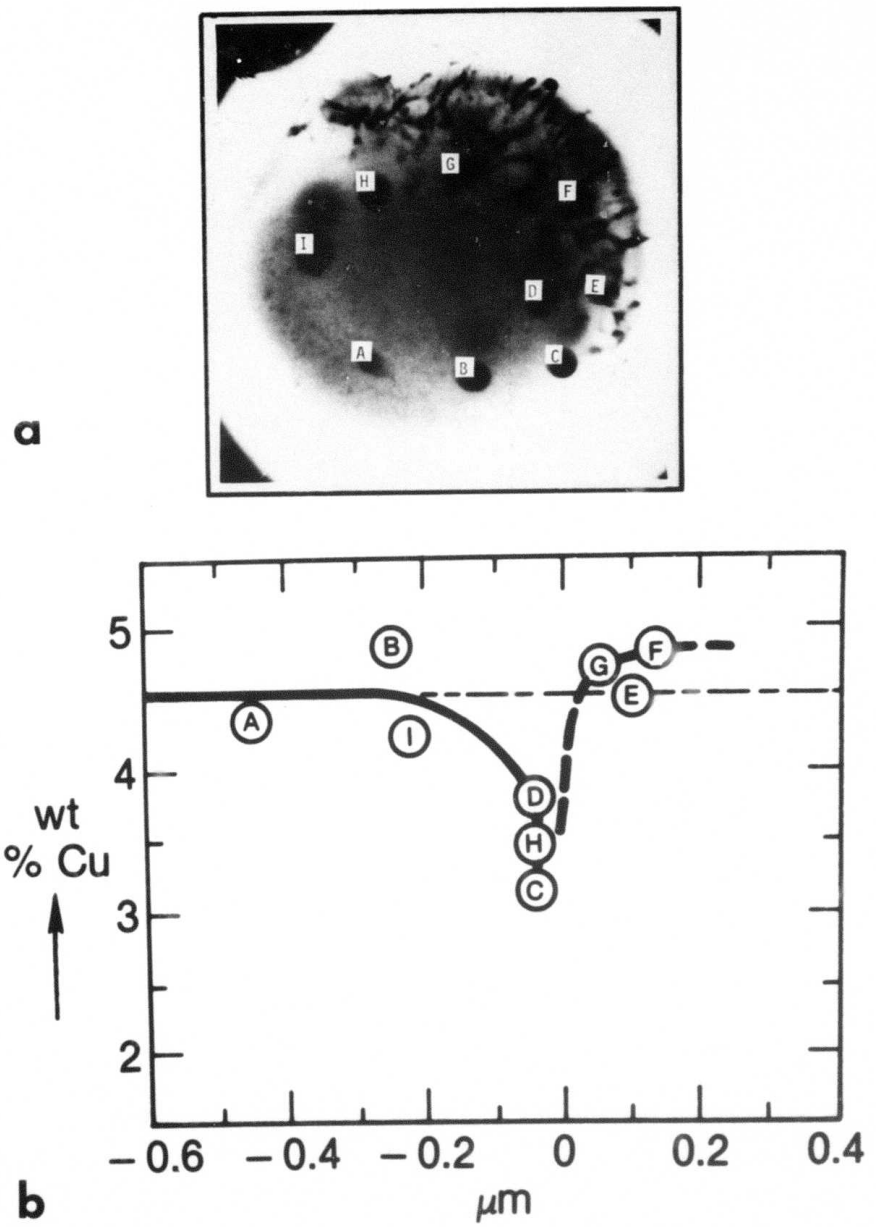

Figure 3. Powder particle (Aℓ 4.5 wt % Cu) (a), and its composition profile (b).

on the 4.5 wt % Cu particle where the microanalysis was performed. It was found that the average composition of the partitionless solidified volume and that of the cell containing volume is the same and equal to the nominal composition of the alloy. The composition of the interface is found to be leaner in Cu. Due to experimental difficulties the exact concentration of Cu in the interface could not be determined, but as the volumes surrounding the interface are richer in Cu it is evident that any error in the composition determination results in higher Cu concentration readings. It is believed, therefore, that the concentration of Cu in the interface is lower than detected.

An example of the results obtained by in situ heat treatment is given in Fig. 4. The particle shown contain 6 wt % Cu and in its original shape it contains cells in about 50% of its volume. When heat treated, two kinds of precipitates appear. The θ' type, which appears in the partitionless solidification volume is composed of thin platelets which lie on the {100} planes and their diameter varies between 50nm and 400nm. The other type forms from the cell boundaries which are richer in Cu. These precipitates also form on the {100} planes and are round, 25nm thick and about 75 nm in diameter.

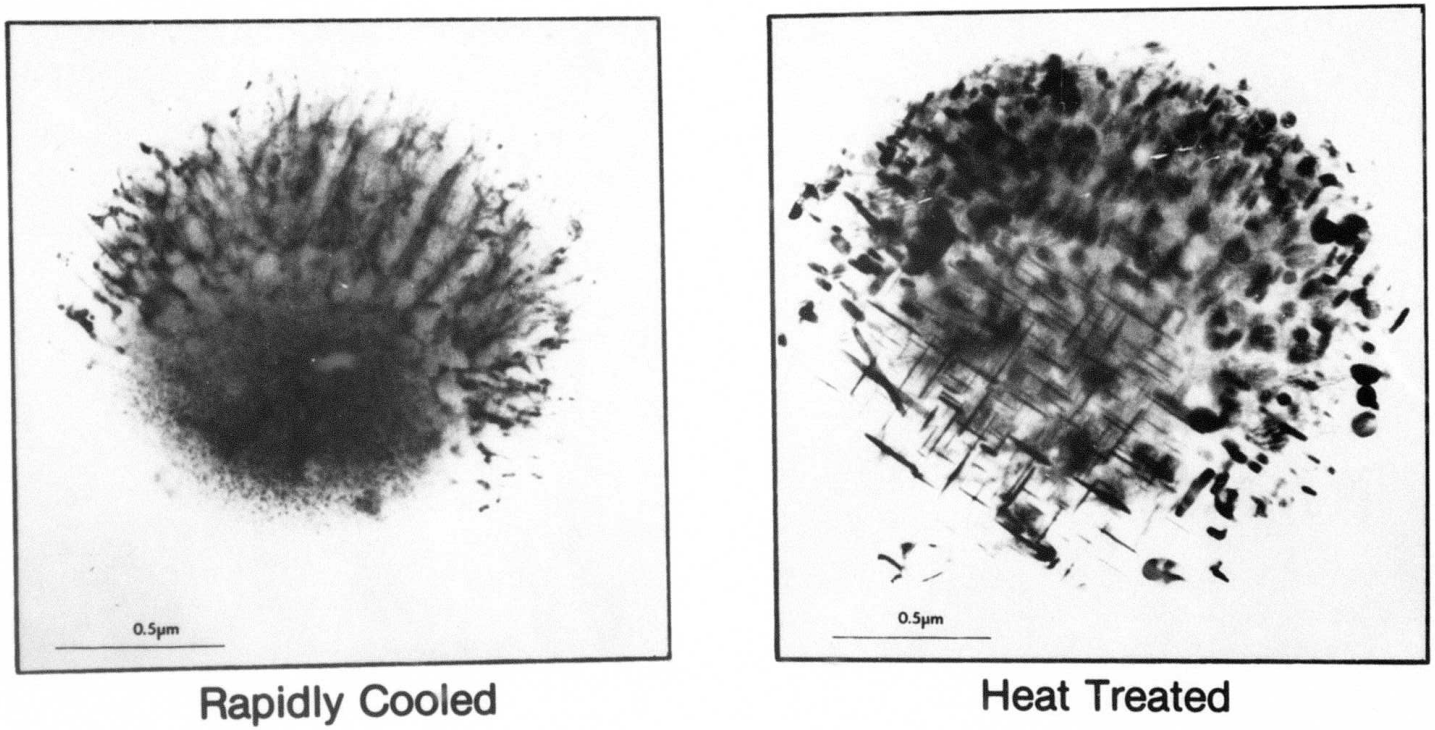

Figure 4. In situ heat treatment of Aℓ-6wt%Cu powder particle.

Discussion

The microstructure obtained in the various particles is governed by their composition, size and the degree of undercooling prior to nucleation. The degree of undercooling of the particles made by the MHD process depends upon the rate of radiation heat loss and, therefore, upon the particle size. Fig. 5 illustrates the solidification process of a particle whose microstructure is characterized by partitionless solidification through the entire particle. Upon cooling the nucleation hypercooling temperature, T_n, is obtained. As the solidification front progresses, the heat of recalescence raises the particles temperature to below T_o and the solidification process is completed. As the particle remains under the T_o temperature through the solidification process the solidification front is stable at all times and partitionless solidification prevails. This can be stated as follows: $(T_o-T_n)Cp \geq \Delta H_m$, where ΔH_m is the heat of fusion.

Another case is illustrated in Fig. 6. In larger particles the heat of recalescence raises the temperature to above T_o $(T_o-T_n)C_p < \Delta H_m)$ and the solidification process is thus divided into two regimes. The first is partitionless solidification as in smaller particles, and the solidification pattern continues until the temperature of the particle rises to T_o. At this point segregation starts, and the building of higher solute concentration at the front results in a depleted zone between the two solidification regimes.

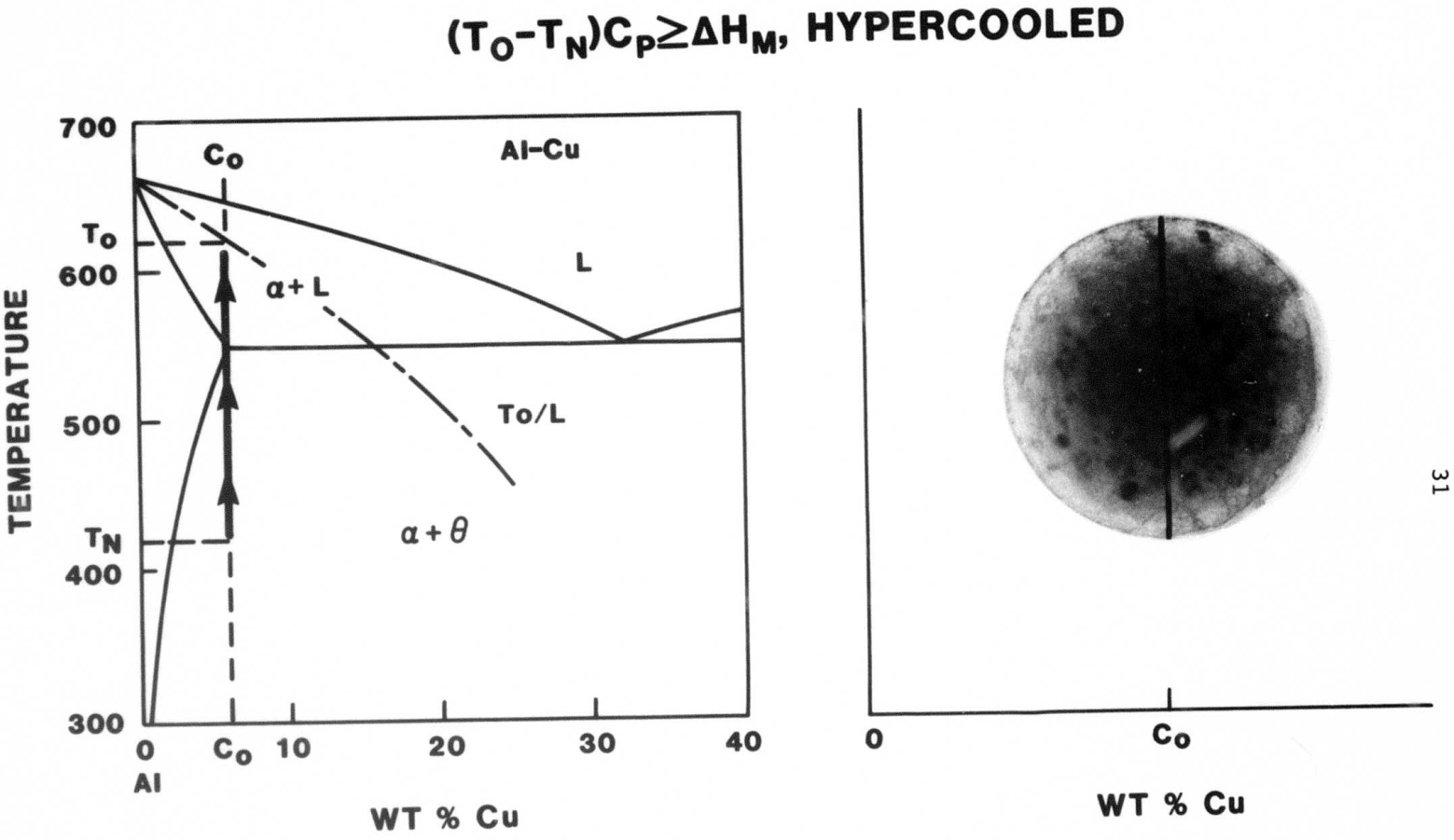

Figure 5. Temperature and composition of the solidification front of a hypercooled particle.

The temperature-composition graph in Fig. 6 and the equivalent composition-distance graph on the particle illustrate the phenomenon. The decrease in the composition at the interface was also detected by the x-ray measurements as described previously but the exact extent of the decrease and its dependence upon the solidification parameters are not yet established.

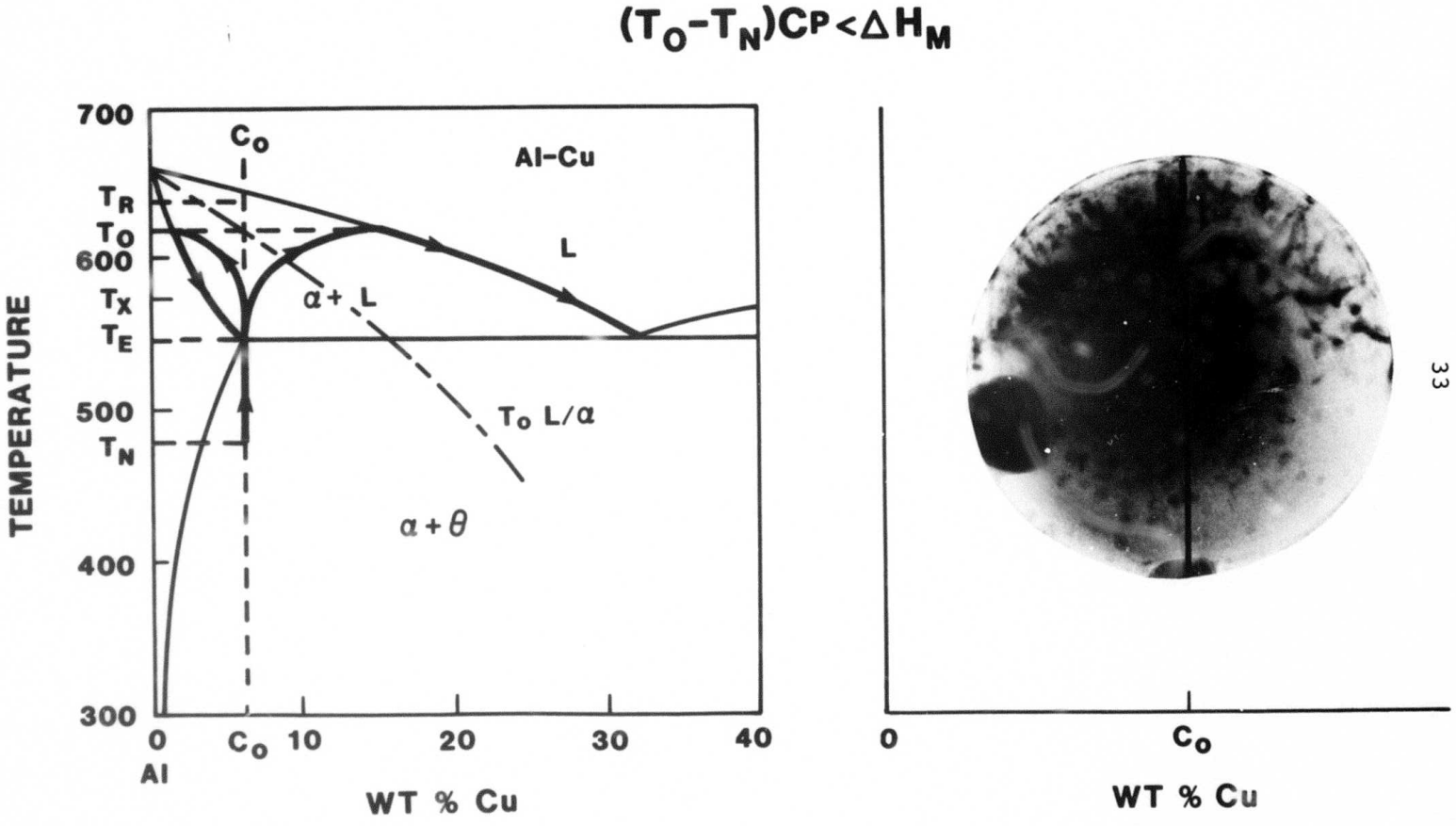

Figure 6. Temperature and composition of the solidification front of a supercooled particle.

References

[1] C. G. Levi and R. Mehrabian, Met. Trans. 13A (1982) p. 13.

[2] J. Perel, J. F. Mahoney, B. E. Kalensher, K. E. Vickers, and R. Mehrabian. "Electrohydrodynamic Generation of Submicron Particles for Rapid Solidification," The Conference on Rapid Solidification Processing Principles and Technology, Reston, Va. (13-16 November 1977), edited by R. Mehrabian, B. H. Kear and M. Cohen (Claitor's Publishing Division, Baton Rouge), 1978, p. 258.

[3] J. Perel, "Electrohydrodynamic Generation of Submicron Particles for Fundamental Rapid Solidification Studies," Invited Talk, Symposium on Melting and Solidification Metals: Theory and Practice, General Electric Corporation R&D, Schnectady, NY (23-24 May 1978).

[4] J. F. Mahoney, B. E. Kalensher, J. Perel and K. E. Vickers, "Development of a Table Top Model for the Generation of Amorphous/Microcrystalline Metal Powders," Interim Report, Office of Naval Research, Arlington, Va. (June 1978).

[5] J. Perel, J. F. Mahoney, B. E. Kalensher, and R. Mehrabian, "Electrohydrodynamic Techniques in Metal Processing," 25th Sagamore Army Materials Research Conference: Recent Advances in Materials Processing, Sagamore Hotel, Bolton Landing, NY (17-21 July 1978), edited by J. T. Burke, R. Mehrabian, and V. Weiss (Plenum Press, New York) 1981, p. 79.

[6] J. Perel, J. F. Mahoney, P. Duwez, B. E. Kalensher and R. Mehrabian, "Applications of Electrohydrodynamics to Rapid Solidification of Fine Droplets and Splats," Second International Conference on Rapid Solidification Processing, Principles and Technologies, Reston, Va. (23-26 March 1980), edited by R. Mehrabian, B. H. Kear and M. Cohen, (Claitor's Publishing Division, Baton Rouge), 1980, p. 287.

[7] J. F. Mahoney, J. Perel, Z. Shanfield, and B. E. Kalensher, "Development of a Tabletop Model for the Generation of Amorphous/Microcrystalline Metal Powders," Interim Technical Report #80-1, Office of Naval Research, Arlington, Va. (July 1980).

[8] J. F. Mahoney, A. T. Forrester, J. Perel and B. E. Kalensher, "Electron Capture in Charged Microdroplet Beams," IEEE/IAS 1980 Annual Meeting, Cincinnati, OH (28 September-2 October 1980).

[9] J. F. Mahoney and J. Perel, "Electrostatic Spray of Silicon for Photovoltaic Applications," IEEE/IAS 1981 Annual Meeting, Philadelphia, Pa. (5-9 October 1981).

[10] Julius Perel and John F. Mahoney, "High Field Purification of Silicon," 160th Meeting Electrochemical Society, Inc. Symposium on Silicon Purification, Denver, Co., Extended Abstracts, p. 1152 (11-16 October 1981).

[11] Julius Perel, John F. Mahoney, Zef Shanfield, Scott Taylor, and Carlos Levi, "An Automated Laboratory Apparatus for the Production of Rapidly Solidified Sub-micron Powders," The Conference on Rapidly Solidified Metastable Materials, Boston, Ma. (17-19 November 1981).

[12] John F. Mahoney, "Tiny Particles Aid Research on Microstructures," Industrial Research & Development, January 1982.

III. Nondestructive Characterization of Rapidly Solidified Aℓ-Mn Alloys

Introduction

This study was performed in collaboration with R. J. Schaefer and R. Mehrabian of NBS and with M. Rosen and J. J. Smith of The Johns Hopkins University. It is one in a series of studies on the Aℓ-Mn system and was partially performed on rapidly solidified ribbons made previously for this program. The importance of studying this system stems from its resemblance to the useful Aℓ-Fe system, and from the fact that phases which are in equilibrium in the Aℓ-Mn system appear as non-equilibrium phases in the rapidly solidified Aℓ-Fe alloys.

Nondestructive methods are needed to characterize the modified layers which can be generated by the action of directed energy sources on the surface of metals. The information generally required includes the depth of the layer and its microstructural character. In many cases the surface layer will not differ in composition from the bulk material, i.e., no surface alloying is present, and the surface layer is detected through the effect of the modified microstructure on the probing signal.

Manganese has a maximum equilibrium solid solubility in aluminum of approximately 1.82 wt.% at the eutectic temperature [1],* which is only slightly below the melting temperature of aluminum. It has long been known [2], however, that this

*See references on p. 48.

solubility can be increased by rapid solidification to compositions far beyond the eutectic (1.95%) between Aℓ and $Aℓ_6Mn$. In response to heat treatment, precipitation may occur as either the equilibrium orthorhombic $Aℓ_6Mn$ or other phases [3] depending upon the temperature and impurity content. Nondestructive evaluation of the state of precipitation may either detect some direct influence of the precipitates or it may primarily detect the decrease of Mn in solid solutions as the process progresses.

Results and Discussion

Sample Preparation

Melt-spun ribbons with Mn concentrations of 0.1, 1, 2, 3, 7, 9, 12, and 15 wt.% Mn were prepared from 99.999% Aℓ and 99.95% Mn. The ribbons were typically 2 mm wide and 20 μm thick. For annealing, the ribbons were sealed in borosilicate glass ampoules with 1/2 atmosphere of helium. Annealing was at 450°C for 5 minutes, 1 hour and 3 hours.

A sample of Aℓ-7 wt.% Mn was prepared for electron beam surface melting by chill casting, rolling at 600°C to a thickness of 9 mm, and annealing for 1 hour at 450°C. Surface melting was carried out by electron beam scans along the length of the sample at a velocity of 50 cm/s, with successive scans offset 0.4 mm laterally and with a time delay of 15 seconds between scans to allow cooling. In this way a rapidly solidified surface layer 8 cm long, 2 cm wide and 0.2 mm deep was formed.

Sample Evaluation

The melt-spun ribbons were evaluated by measurements of lattice parameter, electrical resistivity, and sound velocity, and by transmission electron microscopy. The measurements indicated that at concentrations up to 12wt.% most of the manganese was in solid solution in the as-spun ribbons. At 450°C, precipitation occurs heterogeneously at the grain boundaries at low manganese concentrations and at many more locations throughout the sample at high concentration. As a result, the supersaturation of manganese in the aluminum lattice diminishes rapidly in the high concentration samples but more slowly in the more dilute alloys where longer-range diffusion is required.

Lattice Parameter Measurements

Lattice parameters were measured on an X-ray diffractometer using CuK_α radiation, plotting calculated values for individual peaks against $\Psi = (\cos^2\theta/\sin\theta)$ and extrapolating to $\Psi=0$. In the as-spun ribbons, diffraction peaks were seen only from the aluminum phase at compositions up to 12wt.% Mn, at the lattice parameter (Fig. 1) decreased linearly with increasing Mn content, with a slope in agreement with prior measurements [2,3]. At 15 wt.% Mn, additional peaks, not corresponding to the equilibrium Al_6Mn phase, appeared in the pattern and the lattice parameter of the Al phase indicated a composition of approximately 4 wt.% Mn in solution.

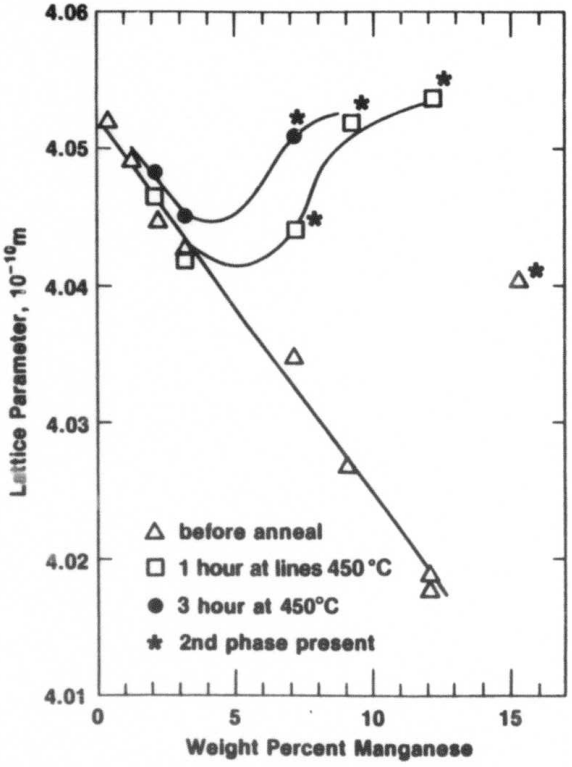

Fig. 1. Variation of the lattice parameter of the Al phase as a function of Mn concentration in the as-spun and annealed conditions.

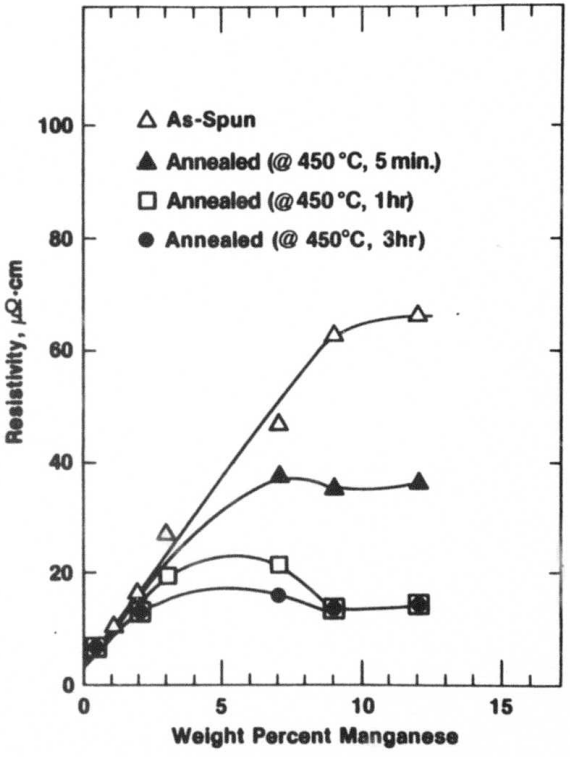

Fig. 2. Variation of the electrical resistivity in Al-Mn alloys as a function of Mn concentration in the as-spun and annealed conditions.

Measurements of the top and bottom surfaces of the 12% alloy showed essentially identical results, indicating that the supersaturated phase was present throughout the thickness of the ribbons.

Annealing of the Aℓ-7wt.% ribbon for 1 hour at 350°C showed little change in the diffraction pattern. After 1 hour at 450°C however, $Aℓ_6Mn$ was present and the peaks from the aluminum phase were significantly broadened, with the average value of the aluminum lattice parameter having increased approximately one half of the way to its equilibrium value at that temperature. At 9 and 12 wt.%Mn, the 1 hour 450°C anneal gave an aluminum phase lattice parameter close to the equilibrium value but at 3 wt.% Mn or less the same anneal gave no perceptible change in the lattice parameter. Annealing for 3 hours brought the lattice parameter of the 7 wt.%Mn sample close to its equilibrium value and also caused significant changes in the low composition samples.

The diffraction chart of a 9 wt.% Mn sample annealed for 5 minutes at 450°C showed extreme line broadening with a line shape indicating that much of the aluminum phase was still close to its original composition but that localized regions had already become significantly depleted in manganese.

The Aℓ-7 wt.% Mn sample prepared for surface melting initially showed a lattice parameter for the aluminum phase that indicated only a small concentration of Mn in solution, and strong $Aℓ_6Mn$ peaks. After electron beam surface melting,

only a single faint peak indicative of a second phase was present and the measured lattice parameter of the aluminum phase lay well below the line for as-spun ribbons, shown in Fig. 1. The value of the lattice parameter in this case, however, may have been seriously affected by the large residual stresses which are inevitably present in such surface melted layers. The surface layer showed a pronounced orientation texture as revealed by the complete absence of the (111) and (222) peaks in the diffraction pattern.

Electrical Resistivity

The electrical resistivity of the ribbons was determined by means of a standard four probe potentiometric method with an accuracy of about 1 part in 10^5. Considering the overall uncertainty in the geometrical shape factor of each sample, the estimated error in the absolute resistivity value is about ±5%. The as-spun ribbons exhibit a strong increase in electrical resistivity with increasing manganese content. An apparent leveling of the resistivity is observed at concentrations above 9 wt.% Mn. Annealing at 450°C, even for short periods (5 minutes), has a large effect on the electrical resistivity of the higher concentration alloys. By means of a nucleation and diffusion controlled process, Al_6Mn_4 particles are precipitated out of the aluminum matrix, thus denuding the lattice of effective scatterers of electrons. This "purification" process is apparently responsible for the observed decrease in electrical resistivity relative to the supersaturated, as-spun, alloy. (See Figure 2).

Electron Microscopy

The microstructures of as-spun and annealed ribbons of the 3 wt.% and 9 wt.% Mn alloys are shown in Fig. 3. The 3 wt.% Mn alloy shows only dislocations in the as-spun condition, and after 1 hour at 450°C it shows a few Al_6Mn precipitates localized at grain boundaries. In the Al-9 wt.% Mn alloy, the as-spun alloy consists of a cellular structure with very fine precipitates at the cell boundaries. It is conjectured that the fine precipitates were formed in the solid state during rapid cooling after solidification. It is not clear whether the fine precipitates are direct precursors of the large ones that form upon annealing at 450°C. After 1 hour at this temperature, the 9 wt.% Mn sample shows abundant Al_6Mn precipitates throughout.

X-ray, TEM and electrical resistivity observations all indicate that at high supersaturations precipitation progresses most rapidly because of the large number of nuclei formed and the correspondingly short diffusion distances. The leveling of the electrical resistivity at concentrations above 9 wt.% Mn may be the result of the presence of the precipitates in the cell boundaries. It is suggested that the concentration of Mn in the Al lattice adjacent to the cell boundaries is very low, and in this case these regions would act as a continuous network of low-resistivity material which would decrease the electrical resistivity of the sample to a larger extent than a simple volume fraction would indicate. The

Al-3 Wt. % Mn

No segragation is observed in the as-spun ribbon. Following heat treatment, large Al_6Mn precipitates form at the grain boundaries.

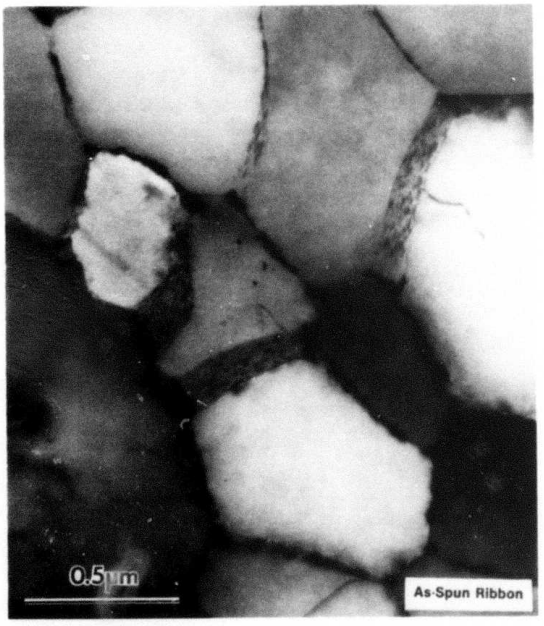

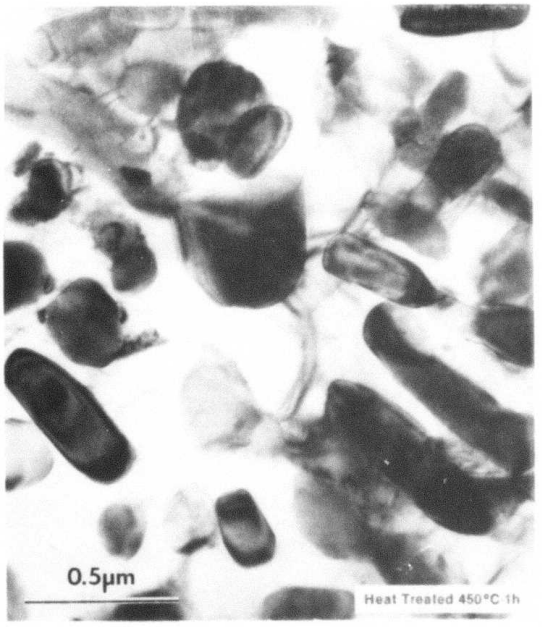

Al-9 Wt. % Mn

Fine particles of metastable compound form at the grain boundaries of as-spun ribbon. Following heat treatment, precipitation of Al_6Mn is observed.

Fig. 3. TEM of Al - 3 wt.% Mn and Al - 9 wt.% Mn in the as-spun and annealed conditions.

x-ray diffraction peaks of the Aℓ-12 wt.% Mn ribbons have distinct tails on the low angle side, confirming that some aluminum is present with considerably less than 12 wt.% Mn in solution.

Sound Wave Velocity

The velocity of ultrasonic, extensional, waves $V_e=(E/\rho)^{1/2}$, where E is the Young's modulus and ρ is the density, propagating along the ribbon was determined by measuring the transit time of a single pulse generated by a laser and detected by a piezoelectric transducer. The detector was about 200 mm from the spot on the ribbon irradiated by the Q-switched Nd:YAG laser (Fig. 4). The transit time of the extensional sound wave propagating along the ribbon could be determined to within one part in 10^5. The separation between the impinging laser pulse and the quartz receiver was determined to within ±0.2 mm. The total estimated error in the calculated value of the sound velocity was ±0.1%. The measurements were carried out at room temperature in the as-spun condition and after the ribbons were subjected to the appropriate heat treatments.

The propagation velocity of Rayleigh surface waves was used to characterize the supersaturated solid solution generated by electron beam surface melting of the slab of Aℓ-7 wt.% Mn. The Rayleigh velocity in the electron beam melted and rapidly solidified layer was found to be 3039 m/s. On the untreated side of the slab, the microstructure of which consisted of $Aℓ_6Mn$ precipitates in an aluminum phase matrix, the Rayleigh wave velocity was 3091 m/s, substantially

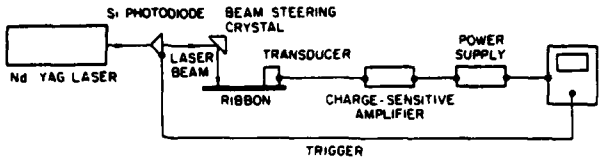

Fig. 4. Laser generation and piezoelectric detection of ultrasonic waves in thin ribbons.

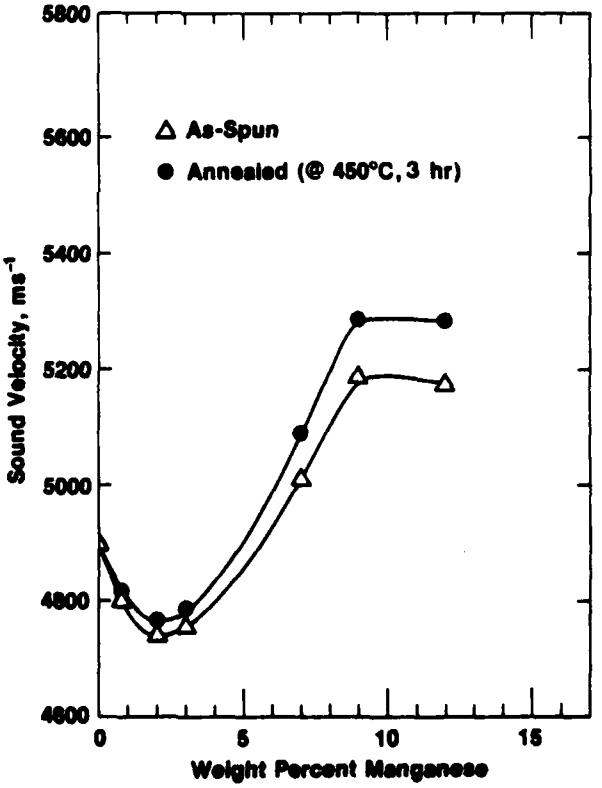

Fig. 5. Variation of the extensional sound wave velocity in Al-Mn alloys as a function of Mn concentration in the as-spun and annealed conditions.

higher than the velocity in the supersaturated solid solution. This behavior was expected since the specific sound velocity of the Al_6Mn particles is substantially higher than that of the aluminum matrix. A similar behavior was observed in Al-Cu alloys after aging [5].

Figure 5 shows the variation of the sound velocity in Al-Mn alloys as a function of Mn content for both as-spun and annealed alloys. The salient feature in Fig. 5 is the fact that the sound velocity, and thus the Young's modulus, of the heat treated alloy is always higher than that of the as-spun state. The difference between the as-spun and the annealed conditions increases with increasing Mn concentration, up to 9 wt.% Mn. This relatively large difference is significant when nondestructive techniques are considered for monitoring on-line and in real-time the progress of the metallurgical process leading to a rapidly solidified single-phase supersaturated alloy.

The extensional sound wave velocity initially decreases with increasing Mn content up to about 2 wt.% Mn. Subsequently the velocity increases, followed by a plateau starting at 9 wt.% Mn. The density, based on the measured lattice parameters of the as-spun ribbons, is expected to be a linear function of composition. Reported values of the static elastic modulus as a function of composition [6] show a slight suggestion of nonlinearity, but not enough to account for the pronounced minimum in sound velocity seen here. Thus, it is apparent that either the density of the melt-spun ribbons differs from

value derived from X-ray measurements, or the elastic modulus of the ribbons differs from that measured statically on bulk samples.

Conclusions

Nondestructive ultrasonic and electrical resistivity measurements were found to be feasible for in-process dynamic monitoring and determination of the supersaturation range of rapidly solidified alloys. Up to 12 wt.% Mn can be incorporated into an Aℓ lattice by rapid solidification, and the subsequent precipitation can be monitored by any of several methods.

References

[1] Metals Handbook Vol. 8, ASM 1973.

[2] G. Falkenhagen and W. Hofman, Z. Metallkunde 43, 69 (1952).

[3] R. Hoier, S. E. Naess, and E. Nes, Z. Metallkunde 64, 640 (1973).

[4] I. Obinata, E. Hata, and K. Yamagi, J. Japan, Inst. Met. 17, 496 (1953).

[5] M. Rosen, E. Horowitz, S. Fick, R. Reno and R. Mehrabian, Mater. Sci. Eng. 53, 163 (1982).

[6] N. Dudzinski, J. R. Murray, B. W. Mott, and B. Chalmers, J. Inst. Metals 74, 291 (1948).

IV. Metastable Phases in Rapidly Solidified Aluminum-Rich Aℓ-Fe Alloys

Introduction

This study is a part of the ongoing effort aimed at the understanding of the phases which are present in Aℓ-Fe rapidly solidified alloys, and their transformation as a function of the heat treatment until the equilibrium phases are formed. The study was performed in collaboration with L. J. Swartzendruber of NBS. Because of the current and potential technological importance of metastable phases in aluminum alloys, rapid solidification of aluminum-rich alloys is being extensively studied. We report here some preliminary results from an examination of the Aℓ-rich side of the Aℓ-Fe phase diagram studied using transmission electron microscopy (TEM) and nuclear gamma-ray resonance (NGR). In the region up to about 41 w/o (25 a/o) Fe, current phase diagrams [1]* indicate the existence of two stable phases, primary α-Aℓ (with a minute amount of iron in solid solution) and $Aℓ_3Fe$. Rapid solidification of Aℓ-Fe alloys within the composition range of these two phases produces a number of metastable phases. Which particular phases form depends on the composition and on the solidification rate [2]. Compositions for this study were selected to extend previous results to higher iron concentrations at higher solidification rates.

*See references on p. 55.

Experimental

The alloys were rapidly solidified by chill block casting on a spinning copper wheel. The ribbons obtained were approximately 2 mm wide and 0.035 to 0.050 mm thick. Thin foils for transmission electron microscopy were prepared using a jet electropolishing unit and standard electrolyte at -40°C. All the ribbons were studied in a scanning transmission electron microscope (STEM). The information obtained included general images of the phase structure, selected area microdiffractions, and x-ray microanalysis of the composition of the main phases. Samples for nuclear gamma-ray resonance were prepared by cutting the ribbons into 6 mm lengths and placing them side by side to form a square approximately 6 mm on a side. The resulting samples had an areal density of ^{57}Fe between 0.05 and 0.1 mg/cm^2.

Results

At 25 w/o Fe (Al_6Fe) and below, only two phases were found in the melt-spun alloys: α-Al solid solution with less than 1 w/o Fe, and an "S" phase with a composition near that of Al_6Fe. The diffraction pattern of the observed "S" phase does not appear to match the diffraction patterns for any of the previously reported aluminum-rich phases (Al_3Fe, Al_xFe, Al_6Fe, Al_9Fe_2, or Al_mFe) which form at lower solidification rates [2-3].

At a composition between 9 and 12 w/o Fe a change in morphology of the melt-spun structure occurs. Below 9 w/o, a cellular structure (see Figure 1) is observed. The cells con-

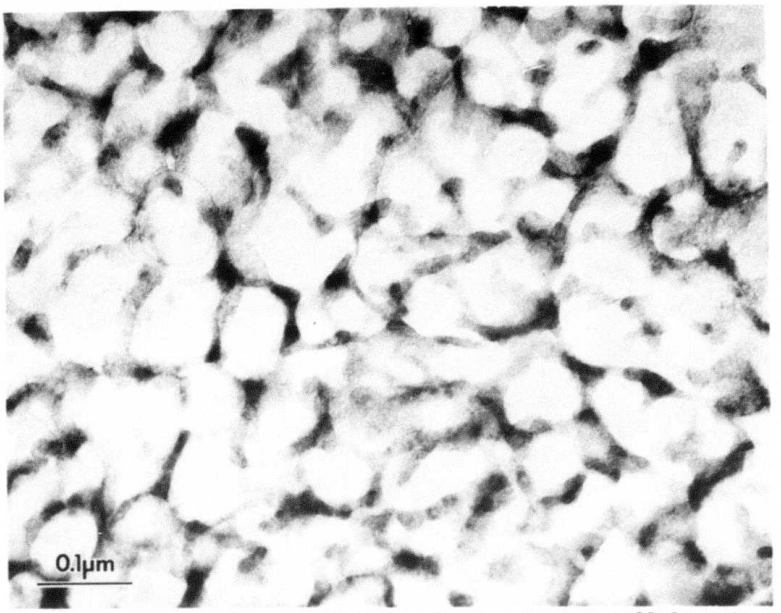

Fig. 1. Micrographs of melt-spun Al-9 w/o Fe showing the cellular structure which forms for alloys with up to 9 w/o Fe. The cells are α-Aluminum with a small amount of iron in solid solution, the cell walls are "S" phase.

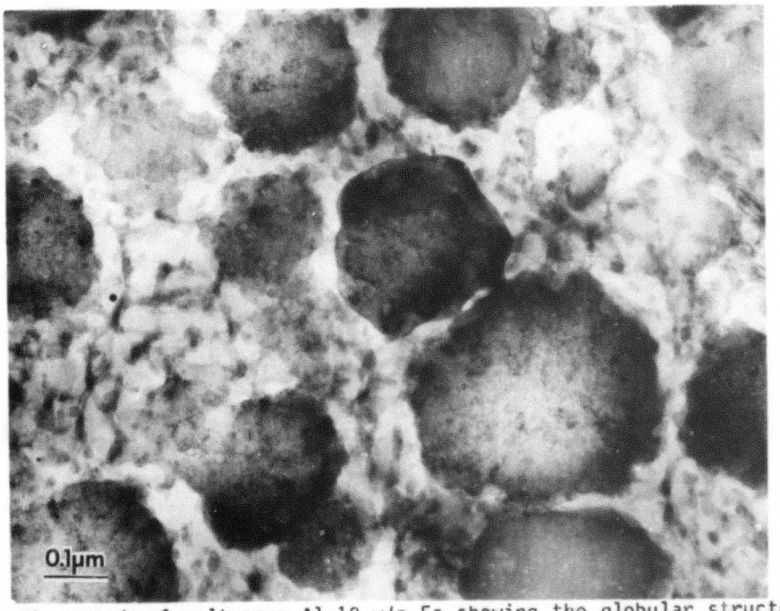

Fig. 2. Micrograph of melt-spun Al-12 w/o Fe showing the globular structure which forms for alloys with 12 or greater w/o Fe. In addition to the globules, a small amount of cellular structure similar to that of Figure 1 can be seen.

sist of α-Aℓ solid solution and the cell boundaries of the "S" phase. Above 12 w/o, a globular phase appears (see Figure 2), with a concomitant decrease in the cellular structure. The globular phase appears to have a crystal structure and a composition identical to the "S" phase at the cell boundaries. At compositions above 25 w/o Fe, $Aℓ_3Fe$ is formed along with the globular "S" phase.

Throughout the range of compositions studied, the NGR spectra consist of three resolved lines. The spectra obtained here, along with previous results [4], indicate that the NGR pattern can be represented as the sum of Lorentzian shaped spectral lines arising from three separate constributions: (1) a nearly symmetric doublet, D, plus a small amount of a singlet S1 (see Figure 3), both from the "S" phase; (2) the same nearly symmetric doublet, D, plus a large amount of the singlet S1, both from $Aℓ_3Fe$; and (3) a singlet S2 from iron in solid solution in α-aluminum. Both the position and relative intensities of the doublet, D, and the singlet S1 are nearly identical for both the "S" phase and $Aℓ_6Fe$. Thus the "S" phase can probably not be distinguished from $Aℓ_6Fe$ by the NGR spectra, however the relative amount of the S1 peak can be used to monitor the transition of the "S" phase to $Aℓ_3Fe$ as the material is heat treated. The position of the doublet D and the singlet S1 from the "S" phase, from $Aℓ_6Fe$, and from $Aℓ_3Fe$ are nearly identical, indicating a very similar local

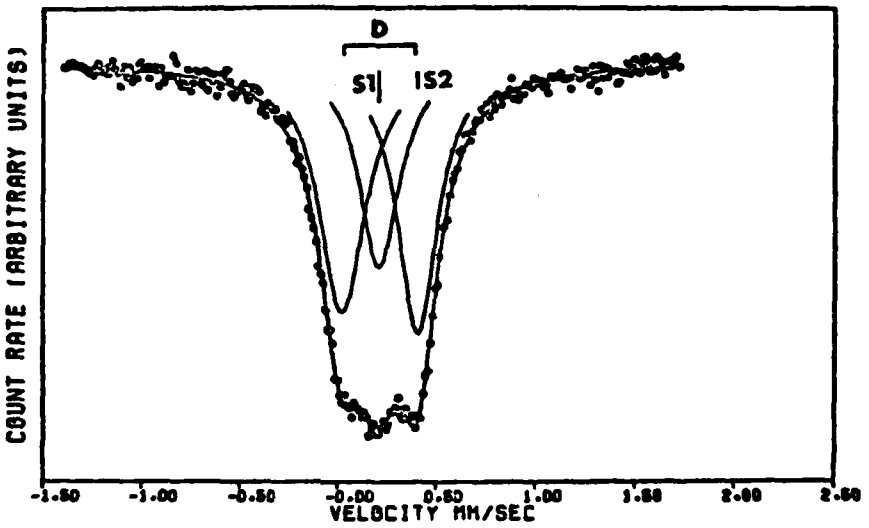

Fig. 3. NGR spectrum from a melt-spun alloy containing mostly Al_3Fe. The spectrum has been analyzed as a symmetric doublet , D, a singlet S1, and a singlet S2. The marking shown indicates the positions of the lines (but not their relative intensities).

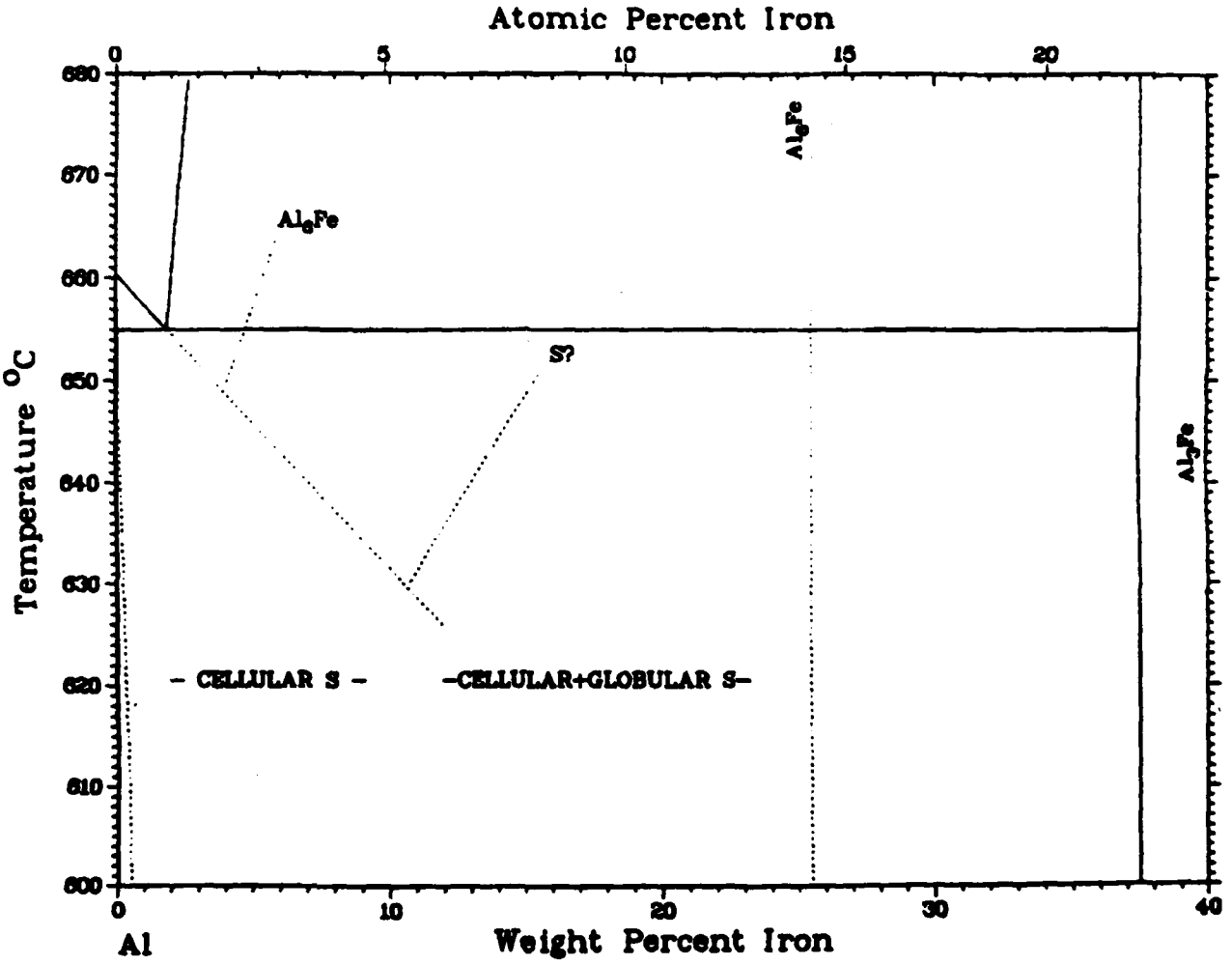

Fig. 4. A hypothetical metastable phase diagram for Aℓ-rich aluminum iron alloys showing the approximate location of the metastable "S" phase eutectic between α-Aℓ solid solution and the $Aℓ_6Fe$ composition of the "S" phase.

structural and electronic environment for the iron atoms in these phases.

A hypothetical metastable phase diagram is shown in Figure 4. The liquidus and solidus have been extended by dotted lines. It is known that the formation of Al_3Fe can be suppressed at low cooling rates and Al_6Fe forms with the approximate eutectic temperature and composition shown. At the high solidification rates achieved in the melt-spun alloys, the formation of Al_6Fe is suppressed and the "S" phase forms. Below the metastable eutectic composition of about 10.5 w/o Fe, the cellular structure is observed in the melt-spun alloys. Between the metastable eutectic and 25 w/o Fe, the cellular and globular "S" are observed. Above 25 w/o Fe only globular "S" and Al_3Fe are observed. Further studies are underway to quantify the phases present, to determine the effect of heat treatment, and to extend the results with ternary additions.

References

[1] M. Hansen and K. Anderko, "Constitution of Binary Alloys," McGraw Hill, New York, 1958, p. 91.

[2] R. M. K. Young and T. W. Clyne, Scripta Met. 15, 1211 (1981).

[3] T. R. Anantharaman, P. Ramachandrarao, C. Suryanarayana, S. Lele, and K. Chattapadhyay, Trans. Indian Inst. of Metals 30, 423 (1977).

[4] C. Janot and H. Gilbert, Phil. Mag. 27, 545 (1973).

V. The Effect of Rapid Solidification Velocity on the Microstructure of Ag-Cu Alloys

Introduction

This study was performed in collaboration with W. J. Boettinger, R. J. Schaefer and F. Biancaniello of the National Bureau of Standards.* The Ag-Cu binary system and the electron beam passes used in this study create a well controlled set up where most parameters are known or can be calculated. Because of the extreme fineness of the microstructural features produced in the study, TEM characterization is vital. The goal of this research is an experimental determination of the solidification velocity required to produce a microsegregation free microstructure in the Ag-Cu model system.

Rapidly solidified crystalline alloys are well known to exhibit a refined scale of microsegregation and interdendritic second phase particles. In some cases this microsegregation and the interdendritic phases can be completely eliminated by rapid solidification. These microsegregation-free structures can occur in alloys with compositions greater than the equilibrium solubility of the primary phase. Such structures provide an ideal starting microstructure for subsequent thermomechanical processing. However, the solidification velocities required to produce these structures are not well known.

*This study was partially supported by DARPA order #3751, "Application of Solidification Theory to Rapid Solidification."

The classic splat-quenching experiments of Duwez, Klement, and Willens [1]* showed by x-ray diffraction that complete solubility of Ag and Cu in the solid state at all compositions could be obtained despite the presence of a solid miscibility gap and eutectic reaction in the phase diagram. Boswell and Chadwick [2] later showed by TEM examination that splat quenched Ag-Cu solidified from the melt as a single solid phase free of microsegregation. Elliott, Gagliano, and Krauss [3] using a pulsed laser, and Copley, et al. [4-6], using a scanned focused laser, showed that super-saturated solid solutions of Ag-Cu could be formed by surface melting and resolidification experiments. The solutions, however, contained a rather unique structure consisting of bands formed parallel to the local solidification interface. Surface melting and resolidification experiments using focused lasers or electron beams permit better control over solidification velocity than other rapid solidification techniques. Such experiments involve no bulk undercooling due to the presence of the alloy substrate and nucleation processes do not therefore play an important role. Also, because the liquid is contained in its own solid, a knowledge of heat transfer coefficients is not required. In these papers no structures are reported which are free of the bands and the velocities at which the transitions of microstructure occur are not described.

*See references on p. 74.

In the present work, a series of electron-beam surface melting experiments have been performed on Ag-rich, Ag-Cu alloys. Such experiments permit a determination of the transition velocity for changes from dendritic or eutectic growth to microsegregation-free solidification. This information permits the evaluation of existing rapid solidification models and points to areas where new models are required. The results and discussion in this paper appear in more detail elsewhere [7].

Experiments

Alloys were prepared by induction melting of 99.99 percent pure components in a graphite crucible under argon and chill casting in a carbon-coated slab mold. Ingots were cold-rolled to 3 mm thick sheets. For the surface melting experiments, the substrate must be prepared with either no microsegregation or microsegregation fine enough to ensure complete mixing during surface melting. Alloys containing 1 and 5 wt.% Cu were homogenized for 20 h at 750°C. Alloys containing 9, 15, and 23 wt.% Cu were surface melted using overlapping electron-beam passes to a depth of $\sim$ 0.5 mm at a scan speed of 3 cm/s. This produces a dendrite arm spacing less than 1 μm. Alloys containing 28.1 wt.% Cu (the eutectic composition) required no pretreatment. Wet chemical analysis of the six alloys yielded compositions of 1.07, 5.49, 9.23, 15.25, 23.50, and 28.61 wt.% Cu. Rapid solidification experiments were performed by single, one-dimensional sweeps of a focused 21 keV, $\sim$ 50 mA, $\sim$ 1 mm diameter

electron beam at speeds between 1.5 and 400 cm/s across the surface of a prepared alloy substrate which was attached to a water-cooled copper block.

Significant effects arise from the change in weld puddle shape as the scan rate is increased. The local solidification velocity is equal to the product of the scan velocity with the cosine of the angle between the scan direction and the local growth direction. Because of this factor, growth velocities even at the top center of the weld puddle for high scan speeds may differ from the scan speed. By examining longitudinal sections through the weld centerline by optical microscopy and assuming that grain boundaries propagate parallel to the growth direction, the angle, θ, between the electron beam scan direction and the growth direction at the top of the weld can be measured. For scan speeds below 30 cm/s, the growth velocity near the weld surface usually differs from the scan speed by 15 percent or less. At velocities of 200 cm/s, the measurements indicated that the growth rate is about one-half of the scan speed.

Results

Figure 1 shows a summary of the microstructure observed at the center of the weld zone near the free surface as a function of the electron beam scan velocity and alloy composition for all experiments performed. The figure is divided into four regions exhibiting four general types of microstructure: (a) dendritic (cellular), (b) eutectic, (c) banded,

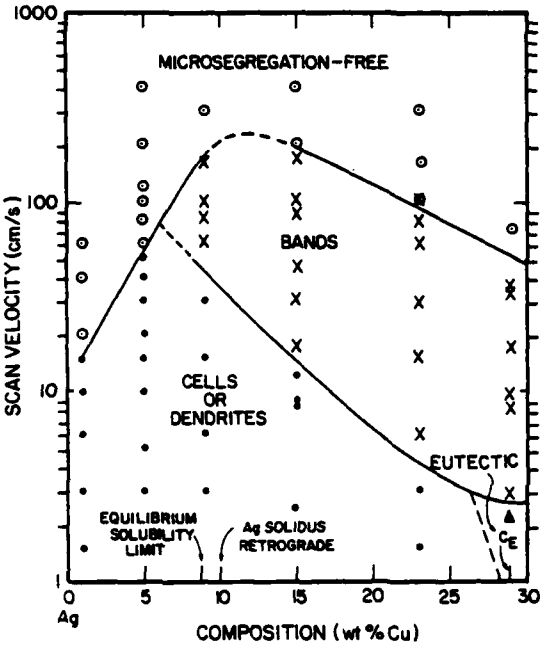

Fig. 1 Summary of microstructures observed in Ag-Cu alloys as a function of composition and electron-beam scan velocity.

and (d) microsegregation-free. The detailed results will be described by alloy composition.

Ag-1 wt.% Cu and -5 wt.% Cu

Dilute alloys exhibit a transition from segregated to microsegregation-free structures at velocities which increase with alloy composition. These velocities agree within a factor of two with the theoretical predictions of absolute stability of the liquid-solid interface as described by Boettinger, et. al. [8].

Ag-9 wt.% Cu, -15 wt.% Cu, and -23 wt.% Cu

These alloy compositions are beyond the equilibrium solubility limit (8.8 wt.%Cu) of Cu in Ag at the eutectic temperature. The 9 wt.% Cu alloy does not exceed a calculated [9] Ag-solidus metastable retrograde composition. As seen in Figure 1, the microstructure of each of these alloys changes with increasing velocity from dendritic to banded and from banded to microsegregation-free.

The maximum velocity at which dendritic growth is observed decreases with alloy composition from 30 cm/s for Ag-9 wt.% Cu to 4 cm/s for Ag-23 wt.% Cu (Fig. 1). The continued refinement of the primary arm spacing with scan velocity for Ag-9 wt.% Cu alloy is shown in Figure 2. The rate of change of spacing with the actual solidification velocity, may, however, be somewhat different due to changes in weld puddle shape as discussed previously. TEM examination of a Ag-15 wt.%Cu melt trail scanned at 2.5 cm/s showed a cellular microsegregation pattern

Effect of Interface Velocity on Fineness of Microstructure

Ag-9wt%Cu

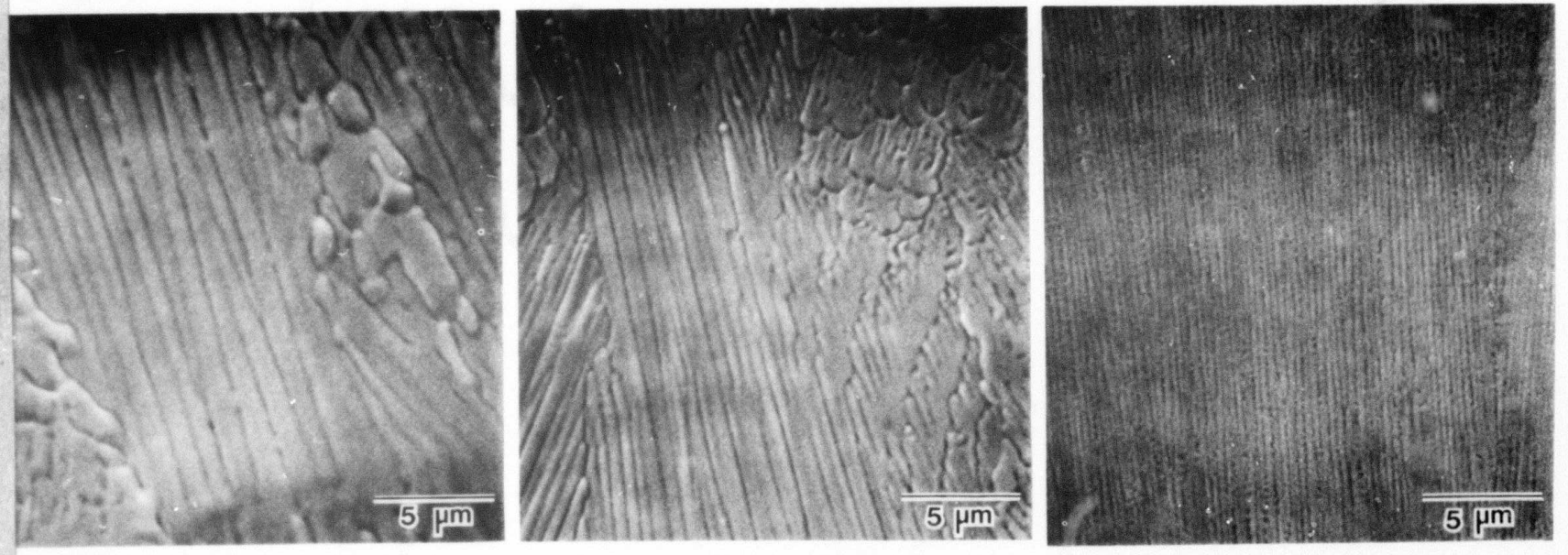

3 cm/s 6 cm/s 15 cm/s

Fig. 2 Refinement of primary dendrite arm spacing with scan velocity for Ag-9 wt.% Cu alloys. SEM.

with a relatively small volume fraction of eutectic in some areas and no eutectic in other areas (Figure 3).

A structure consisting of light and dark etching bands or striations is observed in the intermediate velocity range shown in Figure 1. Figure 4 shows a transverse and a longitudinal section through the weld centerline for a 15 wt.% Cu alloy scanned at 30 cm/s. The lower part of the melted region, where the solidification velocity is lowest, is dendritic. The upper part of the melted region is banded. As seen in Figure 4b the bands adhere to the expected shape of the trailing edge of a melted zone. A transition from dendritic to banded structure, observed in a single sample, suggests strongly that the origin of the banding phenomenon is growth related rather than an artifact of nonsteady beam power [3] or melt convection [5].

TEM examination of the banded structure (Figure 5) in a 23 wt.% Cu alloy scanned at 17 cm/s revealed alternate layers of cellular and cell-free alloy. Evidently the dark etching material seen in optical micrographs of the banded structure corresponds to the cellular layer. X-ray fluorescence measurement in the TEM with a probe size just large enough to average over the entire width of an individual layer ($\sim$ 0.4 μm) revealed no statistically significant difference in average composition of the cellular and cell-free layers. Clearly microsegregation does exist within the cellular layers. Care was taken in the preparation of the TEM sample to document the growth direction.

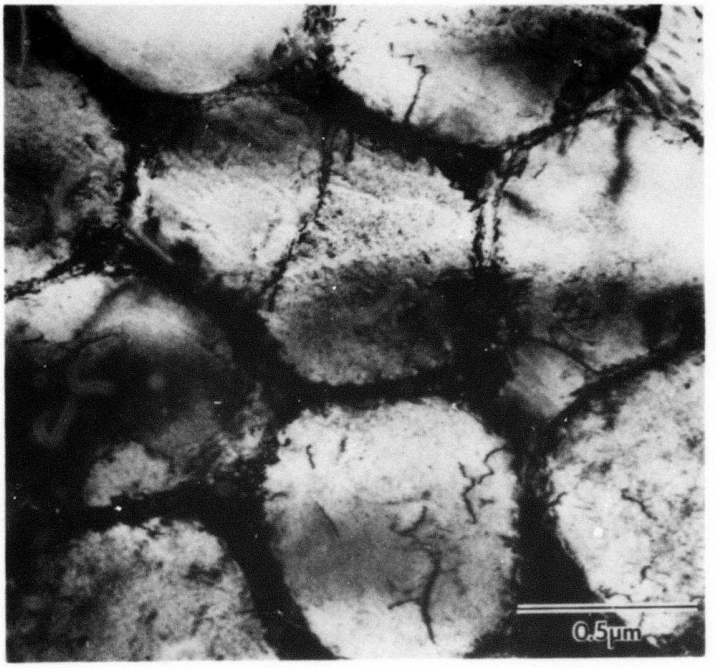

Fig. 3 Cellular microsegregation pattern observed in Ag-15 wt.% Cu alloy at a scan velocity of 2.5 cm/s. TEM.

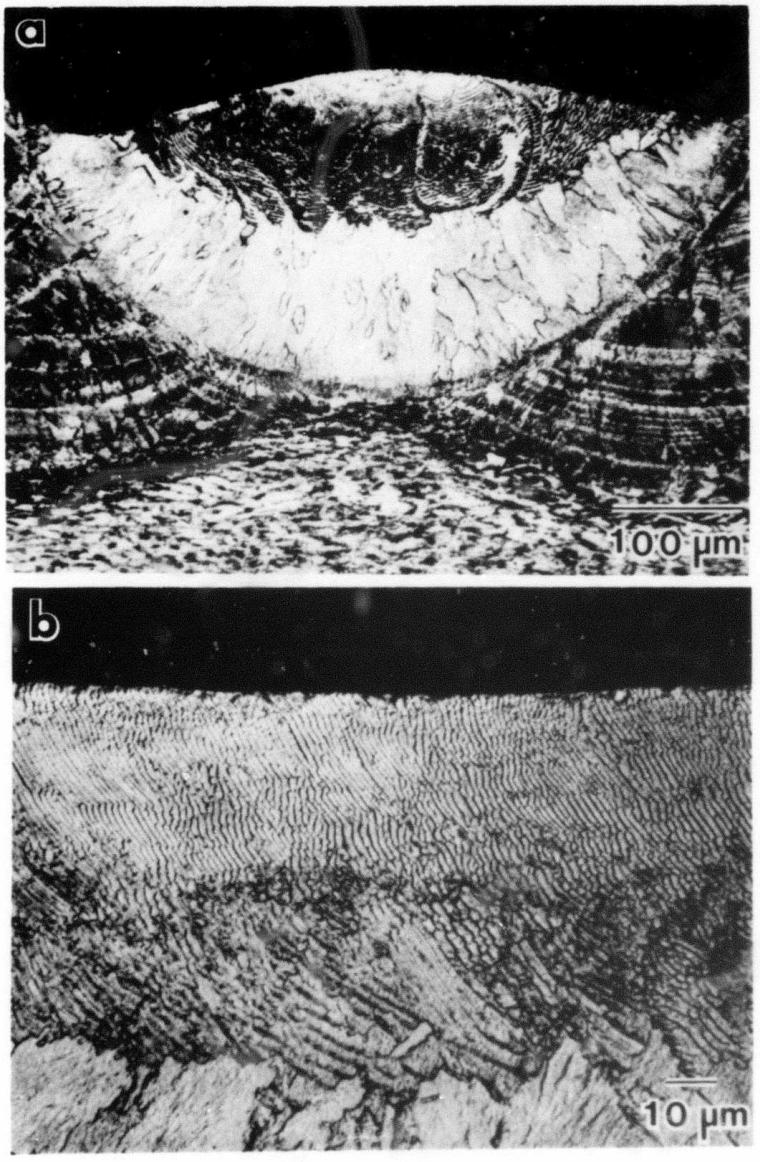

Fig. 4 (a) Transverse and (b) longitudinal sections of a Ag-15 wt.% Cu alloy scanned at 30 cm/s, showing transition from (unresolved) dendritic structure to the banded structure. Optical microscopy. The scan direction is to the right in (b).

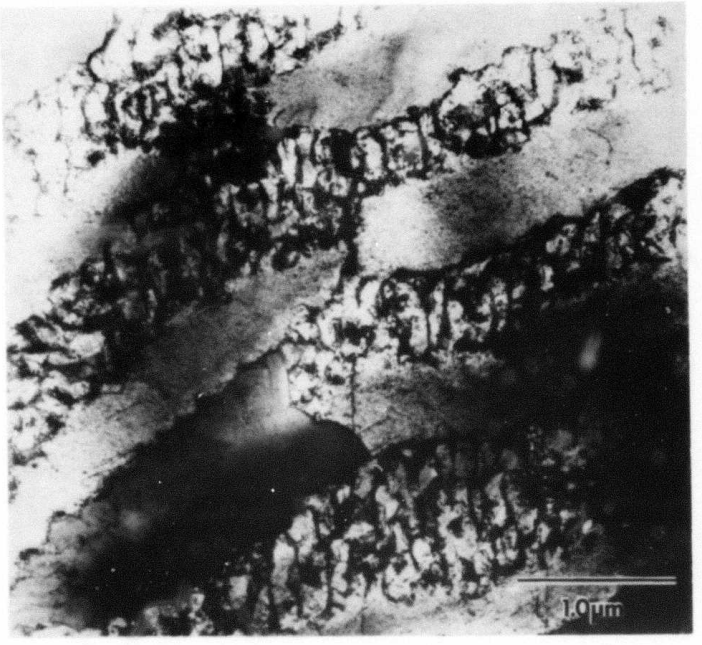

Fig. 5 High magnification view of the banded structure. The growth direction is from lower right to upper left. TEM.

The cellular layer appears to originate microstructurally from an interface instability occurring in the cell-free layer. The cellular structure then propagates for a short distance until a layer of solute marks the cell fronts. The continuity between the cell-free layer and the subsequently formed cellular region is seen clearly in the isolated subgrain (dark grain). For higher scan velocities the width of the cellular layers decrease compared to the width of the cell-free layers, until at high velocity the cellular layers disappear and the banded structure is absent. In eutectic alloys, the banded structure is identical with the exception of a finer cell size.

Coupled Growth

The maximum observed growth rate for the Ag-Cu eutectic in the present work is $\sim$ 2.5 cm/s with a spacing of $\sim$ 200 Å. Cline and Lee [11] have directionally solidified the Ag-Cu eutectic up to a growth rate of 0.27 cm/s with an average lamellar spacing of $\sim$ 950 Å. Growth in their experiments at higher velocities was prevented by the limitations of heat extraction in their solidification furnace. They found the lamellar spacing, λ, and the growth velocity, v, to be related by

$$\lambda^2 v = 1.4 \times 10^{-11} \text{ cm}^3/\text{s}. \quad (1)$$

In the present experiments, the heat extraction rate is not limited by a furnace. Extending their relation to a growth velocity of 2.5 cm/s predicts a lamellar spacing of 237 Å. This compares quite favorably with the eutectic spacing seen in the present work.

The present results strongly suggest that there should exist a theoretical limit on the rate at which coupled eutectic growth can occur. One theoretical limit can be found from the inclusion of a temperature dependent diffusion coefficient in eutectic growth theory [12]. The results of Eq. (1), phase diagram information and diffusion data [13] can be used to show that for slow growth, $v = 3.5 \times 10^{-4}$ (cm s^{-1} K^{-2})ΔT^2, where ΔT is the difference between the interface temperature and the eutectic temperature. Incorporating the temperature dependence of D to extend these relations to large undercooling yields a maximum velocity of a 4.9 cm/s at a spacing of 78 Å. These estimates compare to the experimentally determined values of 2.5 cm/s at 200 Å. Possible reasons for this discrepancy and other theoretical limits on the eutectic growth rate are discussed elsewhere [7].

It should be emphasized that the temperature dependence of the diffusion coefficient only becomes important in the present analysis because of the relatively large undercoolings required to accomplish the solute redistribution and surface area creation necessary for eutectic growth. For dilute alloys this effect is much less important.

It is also interesting to note that the finest spacing seen by Boswell and Chadwick [2] in splat quench alloys was $\sim$ 300 Å. This observation was used by them to assess the growth rate imposed by the splat quench on the foil. Because this eutectic structure occurred only in a small region adjacent

to the metastable extended solid solution, it seems more likely that a maximum growth rate for the eutectic was reached locally and surpassed in most of the foil to form the metastable structure.

Dendritic Growth in Concentrated Alloys

To be consistent with the idea that a temperature dependent diffusion coefficient leads to a maximum rate for coupled growth of a eutectic, a maximum rate for dendritic growth of concentrated alloys must also exist. Although the theory of dendritic growth is continually being refined [14], especially for high rates, a simple expression formulated by Burden and Hunt for controlled growth [15] with the inclusion of a temperature dependent diffusion coefficient demonstrates the qualitative features of this maximum rate for dendritic growth. This calculated maximum velocity [7] parallels the experimental data for the boundary between dendritic and banded microstructure. The calculated values are a factor of 2 to 4 higher than the experimental data, consistent with the disparity between the calculated and observed maxima for eutectic alloys. For very dilute alloys this maximum is irrelevant because it occurs at velocities above those at which the planar interface is stable.

Microsegregation-Free Structure

For Ag-1 wt.% Cu and -5 wt.% Cu alloys, microsegregation free structures are produced by planar growth at velocities predicted by absolute stability theory with equilibrium

partitioning [8]. For concentrated alloys beyond the solidus retrograde composition, equilibrium partitioning is not possible when a microsegregation-free structure is produced. Because the banded structure is eliminated at velocities of the order of 1 m/s where significant solute trapping is expected [8], the transition from banded structure to microsegregation-free structure is most likely related to this phenomenon. The upper velocity boundary of the banded region (Figure 1) when extrapolated to pure Ag suggests a velocity for solute trapping of $\sim$ 5 m/s for dilute alloys. This velocity is consistent with data obtained for solute trapping in dilutely doped Si [16]. The fact that the eutectic composition can be produced as a single phase microsegregation-free material at lower growth rates than, for example, 9 and 15 wt.% Cu alloys, suggests a significant composition dependence for the onset of solute trapping. The 9 wt.% Cu, 15 wt.% Cu, and 23 wt.% Cu alloys are free of the bended structure at velocities of 300, 200, and 157 cm/s and above (Fig. 1). As discussed in a previous paragraph, the exact values of these velocities may not be significant because changes in weld puddle shape at scan velocities over 100 cm/s may lead to significant differences between the scan velocity and the solidification velocity. Clearly, however, the banded structure can be suppressed by high scan velocities to produce a microsegregation-free structure. Furthermore, this velocity decreases with increasing concentration. Figure 6 shows micrographs

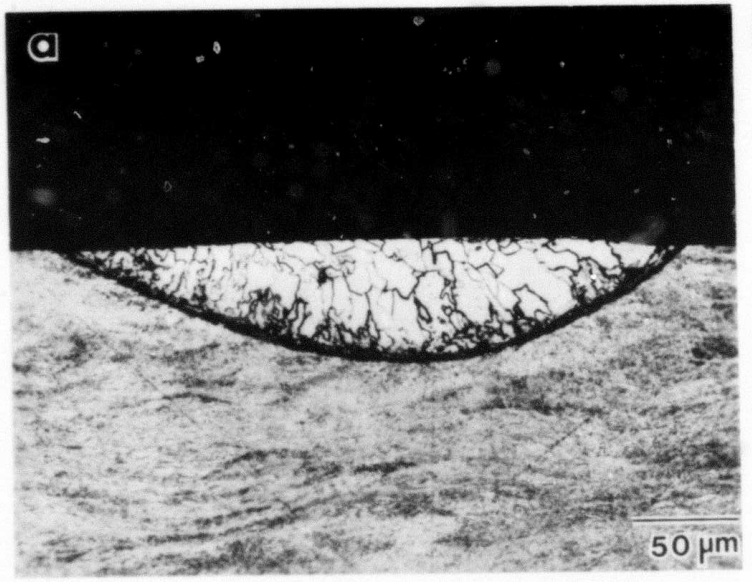

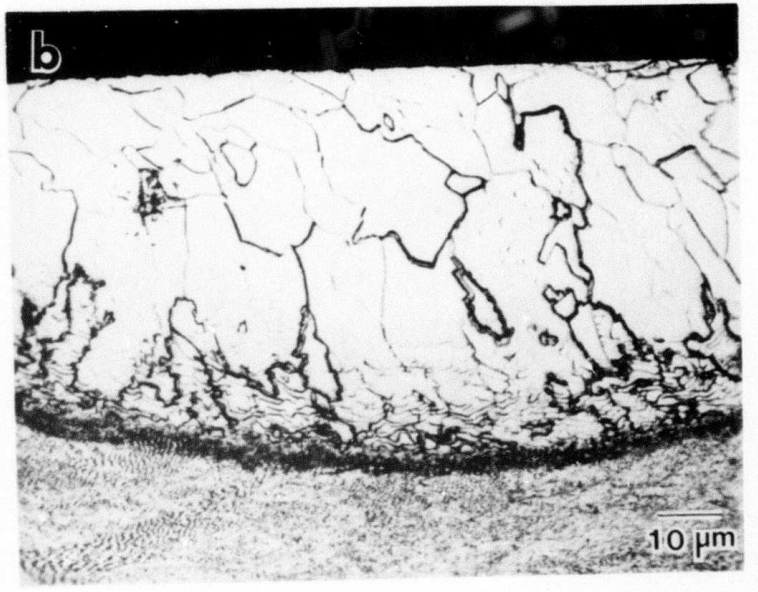

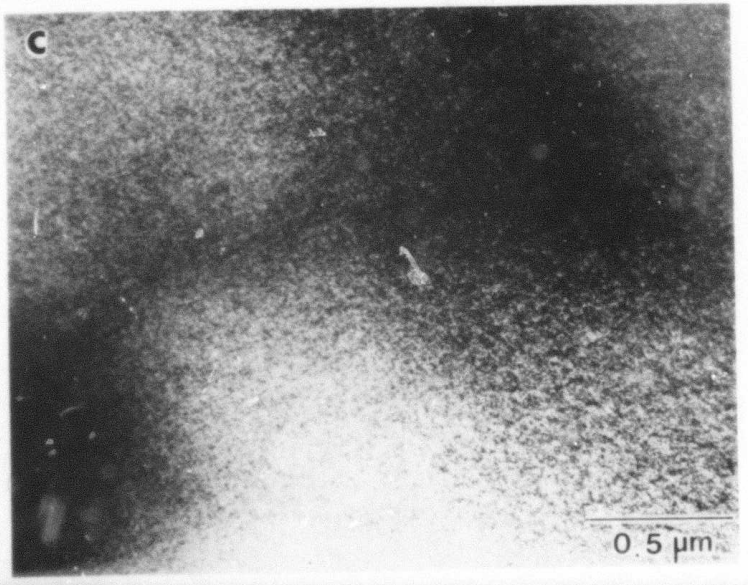

Fig. 6 Microsegregation-free structure obtained in Ag-23 wt.% Cu scanned at 157 cm/s. Note the presence of the banded structure at the bottom of the weld zone in (b) and the presence of spinodal decomposition in (c). (a,b) optical microscopy (severely etched); (c) TEM.

of a 23 wt.% Cu alloy scanned at 157 cm/s. The transition from a banded structure at the bottom of the melted region, where the growth rate is low, to a band-free structure at the top of the melted region, where the growth rate is high, is seen in Figure 6b. TEM micrographs of this sample (Figure 6c) confirm the absence of bands but show significant solid state (spinodal) decomposition of the microsegregation-gree structures produced from the melt.

Ag-28 wt.% Cu

The eutectic composition, when electron beam melted at 2.5 cm/s, consists of a fine eutectic structure with a spacing of $\sim$ 200 Å. The electron diffraction pattern from the eutectic yields lattice parameters of 4.05 Å and 3.65 Å for the two phases. These values are close to those obtained [10] for Ag and Cu at their respective limits of equilibrium solid solubility at the eutectic temperature. Above 2.5 cm/s the eutectic composition does not solidify by a coupled growth mechanism. The microstructure consists of the same banded structure observed for noneutectic alloys. Above 70 cm/s the eutectic composition forms without segregation similar to the structures shown in Figure 6.

Banded Structure

The origins of the banded structure are difficult to determine with certainty. Beck, Copley, and Bass [6] have recently suggested that the bands are due to an instability proposed by Baker and Cahn [17] related to growth with solid

composition and interface temperature above the solidus. However, the observation of band-free structures in alloys for alloy composition beyond the solidus retrograde, where single phase growth can never occur below the solidus, seems to negate this idea.

The preceding discussion has suggested that the lower velocity boundary of the banded region in Figure 1 is caused by a limitation of the maximum growth rate of dendritic and eutectic growth in concentrated alloys. The discussion also has suggested that the upper velocity boundary of the banded region in Figure 1 is caused by significant deviation from interfacial equilibrium and the concommitant increase of the partition coefficient to unity. Clearly the microscopic events which occur during the formation of the banded structure must be related to these two phenomena.

References

[1] P. Duwez, R. H. Willens, and W. Klement, Jr., J. Appl. Phys. 31, 1136 (1960).

[2] P. G. Boswell and G. A. Chadwick, J. Mat. Sci. 12, 1879 (1977).

[3] W. A. Elliott, F. P. Gagliano, and G. Krauss, Met. Trans. 4, 2031 (1973).

[4] S. M. Copley, M. Bass, E. W. Van Stryland, D. G. Beck, and O. Esquivel, Proc. III Int. Conf. Rapidly Quenched Metals, 1, p. 147, The Metals Society, London (1978).

[5] D. G. Beck, S. M. Copley, and M. Bass, Met. Trans. A 12A, 16 (1981).

[6] D. G. Beck, S. M. Copley, and M. Bass, Met. Trans. A 13A, 1879 (1982).

[7] W. J. Boettinger, R. J. Schaefer, F. Biancaniello, and D. Shechtman, Met. Trans. A., to be published.

[8] W. J. Boettinger, S. R. Coriell, and R. R. Sekerka, these proceedings.

[9] J. M. Murray, Met. Trans. A, (1983) to be published.

[10] R. K. Linde, J. Appl. Phys. 37, 934 (1966).

[11] H. E. Cline and H. Lee, Acta Met. 18, 315 (1970).

[12] W. J. Boettinger, in Rapidly Solidified Amorphous and Crystalline Alloys, B. H. Kear, B. C. Giessen, and M. Cohen, Eds., Elsevier, p. 15 (1982).

[13] T. Yamamura and T. Ejima, J. Jap. Inst. Met. 37, 901 (1973).

[14] R. Trivedi, to be published.

[15] M. H. Burden and J. D. Hunt, J. Cryst. Growth 22 109 (1974).

[16] M. J. Aziz, J. Appl. Phys. 53, 1158 (1982).

[17] J. C. Baker and J. W. Cahn, in Solidification, ASM, Metals Park, p. 23 (1971).

Acknowledgement

We wish to express our appreciation to the following staff of the National Bureau of Standards for their cooperation and collaboration on various aspects of this research program; Frank S. Biancaniello, William J. Boettinger, S. R. Coriell, Robert Mehrabian, S. D. Ridder, R. J. Schaefer, L. J. Swartzendruber; to T. Z. Kattamis of the University of Connecticut, and to M. Rosen and J. J. Smith of The Johns Hopkins University.

APPENDIX 1. LIST OF PUBLICATIONS

1. D. Shechtman and L. J. Swartzendruber, "Metastable Phases in Rapidly Solidified Aluminum-Rich Aℓ-Fe Alloys," Proceedings of the Materials Research Society, Boston, Mass., November 1982.

2. D. Shechtman, S. D. Ridder, and R. Mehrabian, "The Structure of Microparticles Made by the MPP Technique," Proceedings of The Third Conference on Rapid Solidification Processing: Principles and Technologies, Gaithersburg, Md., December 1982.

3. W. J. Boettinger, R. J. Schaefer, D. Shechtman and F. Biancaniello, "The Effect of Solidification Velocity on the Microstructure of Ag-Cu Alloys," Proceedings of The Third Conference on Rapid Solidification Processing: Principles and Technologies, Gaithersburg, Md., December 1982.

4. D. Shechtman, T. Z. Kattamis, F. S. Biancaniello, and W. J. Boettinger, "The Microstructure of Rapidly Solidified NiAℓ-Cr Quasibinary Eutectic," Proceedings of The Third Conference on Rapid Solidification Processing: Principles and Technologies, Gaithersburg, Md., December 1982.

5. R. J. Schaefer, M. Rosen, J. J. Smith, D. Shechtman, and R. Mehrabian, "Nondestructive Characterization of Rapidly Solidified Aℓ-Mn Alloys," Proceedings of The Third Conference on Rapid Solidification Processing: Principles and Technologies, Gaithersburg, Md., December 1982.

6. W. J. Boettinger, R. J. Schaefer, F. Biancaniello, D. Shechtman, "The Effect of Rapid Solidification Velocity on the Microstructure of Ag-Cu Alloys," Proceedings of ASM Meeting, Atlanta, Ga., March 1983.